

Article

Experimental and Theoretical Investigation of Single-Slope Passive Solar Still with Phase-Change Materials

Ewelina Radomska ^{1,*}, Łukasz Mika ¹, Karol Sztekler ¹, Wojciech Kalawa ¹, Łukasz Lis ¹, Kinga Pielichowska ², Magdalena Szumera ³ and Paweł Rutkowski ³

- ¹ Department of Thermal and Fluid Flow Machines, Faculty of Energy and Fuels, AGH University of Science and Technology, Mickiewiczza 30 Av., 30-059 Kraków, Poland
- ² Department of Biomaterials and Composites, Faculty of Materials Science and Ceramics, AGH University of Science and Technology, Mickiewiczza 30 Av., 30-059 Kraków, Poland
- ³ Department of Ceramics and Refractories, Faculty of Materials Science and Ceramics, AGH University of Science and Technology, Mickiewiczza 30 Av., 30-059 Kraków, Poland
- * Correspondence: radomska@agh.edu.pl

Abstract: Many attempts are made worldwide to create cheap, efficient, and eco-friendly water desalination systems. Passive solar stills (SS) are considered to be such. This paper presents the results of the experimental and theoretical investigation of the effects of using phase-change materials (PCM) on the performance of SS. The experiments were conducted for two paraffin waxes, as PCM and 1.0, 2.5, and 5.0 kg of PCM were used. The results of the experimental studies were used to validate a mathematical model, which was based on the energy balance ordinary differential equations. The equations were solved numerically since the approximate solutions obtained numerically are sufficient and relatively simple as compared to the exact analytical solutions. A theoretical analysis was then carried out and a novel and detailed dependence on the water evaporation rate as a function of water temperature and the difference between water and cover temperature was determined. It was also found that the productivity of the SS with PCM strongly depends on the operating conditions. For uniform initial temperatures of the SS, its productivity decreases with an increasing PCM-to-water mass ratio, and the maximum decrease is 10.8%. If the SS is not thermally insulated, the PCM can take the role of a thermal insulator and increase productivity by 1.1%, but there is an optimal PCM-to-water mass ratio. The greatest increase in productivity, by up to 47.1%, can be obtained when the PCM is heated outside the SS and inserted into the SS when the water temperature starts to decrease. In this case, the productivity increases with the increasing PCM-to-water mass ratio. These outcomes fill a knowledge gap caused by a lack of justification for why in some cases, the application of PCM fails to improve the productivity of SS.

Keywords: desalination; distillation; paraffin wax; phase-change materials; solar still



Citation: Radomska, E.; Mika, Ł.; Sztekler, K.; Kalawa, W.; Lis, Ł.; Pielichowska, K.; Szumera, M.; Rutkowski, P. Experimental and Theoretical Investigation of Single-Slope Passive Solar Still with Phase-Change Materials. *Energies* **2023**, *16*, 1188. <https://doi.org/10.3390/en16031188>

Academic Editors: Karunesh Kant and Atul Sharma

Received: 7 January 2023

Revised: 16 January 2023

Accepted: 18 January 2023

Published: 21 January 2023



Copyright: © 2023 by the authors. Licensee MDPI, Basel, Switzerland. This article is an open access article distributed under the terms and conditions of the Creative Commons Attribution (CC BY) license (<https://creativecommons.org/licenses/by/4.0/>).

1. Introduction

Probably no one needs convincing how important drinking water and free access to it is for humanity. Drinking impure and saline water can lead to various medical problems, including cholera, polio [1], increased risk of hypertension, as well as skin and diarrheal diseases [2]. The World Health Organization estimates that by 2025, 50% of the population will be living in water-stressed areas [1]. This is the result of an increasing population, the uneven distribution of water resources, and the fact that approximately 97% of the Earth's water resources are saline water [3]. Therefore, water desalination is necessary and the number of water desalination plants has been growing since the 1960s to reach the number of 15,906 in 2018 [4].

Existing water desalination plants are based mostly on reverse osmosis (RO) and multi-stage flash (MSF) distillation. Generally, RO and MSF desalination plants are large-scale and high-capacity units that require large capital expenditure. Nevertheless, building

large-scale desalination plants or delivering water by pipelines or trucks in some areas may be uneconomical and challenging. Therefore, the use of solar stills to desalinate water in such cases appears to be a reasonable alternative.

Passive SS are devices of simple construction with a lack of moving parts and additional energy sources, and they do not require significant capital expenditure [5]. The water obtained in the SS is free of salt and other non-volatile compounds [6]. However, the main drawback of SS is low productivity, usually less than 5 L/m²/day [7]. Therefore, there is a lot of effort spent on improving the productivity of SS.

The main driving force behind the water evaporation process, and hence SS productivity, is the temperature difference between water and cover ΔT [8], and the water temperature, T_w [9]. Tsilingiris [10] reported that as the ΔT increases from 5 to 10 °C, the productivity increases by a factor of 2.6, while for a fixed ΔT , an increase of the SS temperature by 20 °C leads to productivity improvement by a factor of 3.2. Therefore, the methods of increasing the productivity of SS can be divided into two groups: increasing the temperature of the water and decreasing the temperature of the cover [11]. The first way includes, for example: implementing the internal [12] or external [13] reflectors to increase the incident solar irradiance on the water and absorber, or coating the absorber with TiO₂ nanoparticles to increase its absorptivity [14]. On the other hand, decreasing the temperature of the cover can be realized by using the flow of cold water over the cover [15], applying radiative cooling [16], or using an additional external condenser [17].

Based on the above reflections, it appears that desalinating water in SS would be more effective, in terms of productivity, if it was conducted at night when the temperature of the ambient air is low. Therefore, thermal energy storage materials have been proposed to be used in SS to store the excess heat during the day and release it during the night [18]. Among the group of thermal-energy storage materials, phase change materials (PCM) are of great interest for use in SS [19,20]. PCM are materials that undergo reversible phase transitions, most commonly solid-liquid, during which the PCM stores thermal energy in the form of latent heat.

Yousef and Hassan [21] reported that using paraffin wax as PCM can increase the SS daily productivity by 9.5%. Chaichan and Kazem [22] investigated experimentally the performance of SS without PCM (paraffin wax), with pure paraffin wax, and with paraffin wax doped with Al₂O₃ nanoparticles. It was found that the daily productivity of SS with pure paraffin wax and with paraffin wax doped with Al₂O₃ was greater than the productivity of SS without PCM, by 14.3%, and 60.5%, respectively. A similar finding was reported by Kabeel et al. [23], who used pure paraffin wax and paraffin wax with different mass fractions of graphite nanoparticles in the SS. The results showed that the productivity of SS with pure paraffin wax, and with paraffin wax doped with graphite nanoparticles (20% mass fraction) increased by 62.6%, and 94.5%, respectively, compared to the SS without paraffin wax. Furthermore, it was concluded that the productivity of SS increased with the increasing mass fraction of graphite nanoparticles in the paraffin wax. The addition of high thermal conductive nanoparticles into the PCM increases the thermal-conductivity of the latter and intensifies the heat transfer, leading to faster melting and solidification [24].

In the works cited in the above paragraph, the researchers investigated only one PCM-to-water mass ratio. However, the PCM-to-water mass ratio in SS is an issue that has been investigated by several researchers. Shalaby et al. [25] tested the SS without, and with 18 kg of paraffin wax as PCM. The PCM-to-water mass ratio was changed by using 25, and 35 kg of water. The daily productivity of SS without PCM and with 25 kg of water was 3.36 kg/m²/day, while the productivity of the SS with PCM and 25, and 35 kg of water was 3.76, and 2.22 kg/m²/day, respectively. A similar experimental and theoretical investigation, using the Dunkle model, was conducted by Sonker et al. [26], who used 1.3 kg of lauric acid, stearic acid, and paraffin wax as PCM. The depth of water in the SS was changed from 1 to 5 cm. It was reported that the productivity of the SS with paraffin

wax was greater than when the lauric and stearic acids were used. Additionally, the daily productivity decreased with the decreasing PCM-to-water mass ratio.

As can be seen, one way to investigate the PCM-to-water mass ratio is by changing the mass of water, and, in such cases, the productivity of SS increases with the increasing PCM-to-water mass ratio. On the other hand, Mousa et al. [27] used tricosane as PCM in their research, and the PCM-to-water mass ratio was 0.17, 0.24, and 0.51. The PCM-to-water mass ratio was set by varying the mass of the PCM while keeping the mass of water constant. The results showed that the daily productivity of the SS was 627, 630, 545, and 550 mL for the SS with 0 (without PCM), 0.17, 0.35, and 0.51 PCM-to-water mass ratios, respectively. Thus, only in one case (0.17 mass ratio) was the application of PCM advantageous, in terms of improving productivity by 0.5%. The authors justified this result by the fact that as a large amount of PCM is present in the SS, a lot of energy is used to heat and melt the PCM. Consequently, the temperature of the water, as well as the productivity, decreases. On the other hand, Al-Harashseh et al. [28] investigated the SS coupled with solar collector, cover cooling, and different masses of PCM. The maximum productivity improvement was obtained for the maximum investigated PCM-to-water mass ratio of 0.38, and the improvement was 19.0%, compared to the SS without PCM.

Mousa and Gujarathi [29] investigated theoretically, using the Dunkle model, the effects of PCM mass on the productivity of the SS. As the mass of the PCM increased, more heat from the solar radiation was used to raise the PCM temperature and melt it, at the expense of reducing the energy input to the water and increasing the water temperature. As a result, the productivity of the SS decreased with an increasing mass of the PCM. Kateshia and Lakhera [30] investigated the influence of both the water mass and PCM mass on the performance of SS. It was reported that the productivity increased with decreasing water mass and increasing PCM mass.

Another interesting finding was reported by Tabrizi et al. [31] and Sarhaddi et al. [32], who concluded that using the PCM in SS is more beneficial during cloudy than sunny days. Tabrizi et al. [31] reported an increase of 61.9% in productivity when the PCM was used on a cloudy day, but a decrease of 5.6% was observed after applying the PCM on a sunny day. This finding was confirmed further in the theoretical analysis carried out by Sarhaddi et al. [32]. They observed a productivity improvement of 28.6% after applying the PCM during a cloudy day and a productivity reduction of 6.0% after applying the PCM during a sunny day.

Based on the literature review presented above, it can be concluded that:

- PCM can improve the productivity of SS from 0.5% to nearly 100%, but a productivity reduction was also reported in some works, which was also confirmed in the recent review paper by Fu et al. [33];
- The PCM-to-water mass ratio impacts the performance of SS;
- The productivity of SS increases with an increasing T_w and ΔT .

However, there are still some knowledge gaps that need to be filled:

- The conditions under which the PCM improve and under which they reduce the productivity of SS, have not yet been established;
- The optimal PCM-to-water mass ratio remains unclear;
- The water evaporation rate in the function of T_w and ΔT has not been dealt with in depth.

Therefore, this paper aims at filling the abovementioned research gaps by:

- Investigating the impact of the PCM-to-water mass ratio on the performance of the passive SS, depending on the operating conditions;
- Determining the conditions that must be met for PCM to improve the productivity of SS;
- Establishing the evaporation rate of water in the function of T_w and ΔT in the entire range of operating temperatures of the SS.

This paper presents the results of the experimental and theoretical studies on the performance of passive single-slope SS with two different PCM, a variable PCM-to-water mass ratio, and in four operating conditions. Moreover, a comprehensive analysis of the impact of T_w and ΔT on the water-evaporation rate is conducted. Additionally, the following aspects make this paper original, compared to the previously published papers:

- The experiments were conducted in laboratory conditions, which allowed the minimization of the influence of atmospheric conditions on the measurement results;
- The heat- and mass-transfer phenomena occurring in the SS were described by a mathematical model that has not been widely used so far;
- The PCM were placed in flexible plastic bags, which, according to the best of the authors' knowledge, has not been done before in the field of solar stills;
- This is the first time that the SS has been investigated in Poland.

2. Materials and Methods

2.1. Experimental Setup

The effects of using PCM on the performance of the SS were investigated at the experimental setup located at the AGH University of Science and Technology in Kraków, Poland. The experimental setup consisted of a passive single-slope SS equipped with appropriate measuring devices. A detailed description of the experimental setup can be found in the authors' previous paper [34].

The SS, 1.0 m long and 0.5 m wide, was made of a stainless steel sheet and a cover with a glass lid. For the experiments without PCM, four electric heaters were placed directly on the absorber to simulate the solar radiation, as the experiments were conducted under laboratory conditions. However, in the case of using PCM, the bags filled with PCM were placed on the absorber, and then the heaters were placed on the PCM, as shown in Figure 1. Two different commercially available paraffin-waxes were used as PCM. The paraffin waxes were selected due to their appropriate melting temperature and high latent-heat of fusion. Additionally, paraffin waxes are considered to be non-toxic, have good thermal and chemical stability, little supercooling, and are reasonably priced [35].

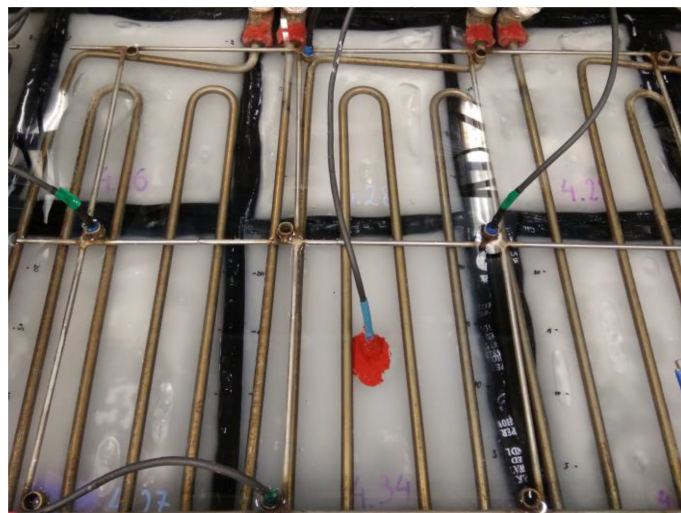


Figure 1. Bags (Type 1) filled with the phase-change materials and placed in the solar still under the electric heaters.

Depending on the mass of PCM used in the experiments, two types of PCM bags were used, namely, Type 1, and Type 2. Each Type 1 bag was filled with 0.50 kg of PCM and its dimensions were $0.23 \times 0.18 \times 0.017$ m. The dimensions of Type 2 bags were $0.145 \times 0.040 \times 0.017$ m and each bag contained 0.05 kg of PCM. Type 2 bags were used during the measurements with 1.0 kg of PCM in the SS, while Type 1 bags were used during the measurements with 2.5 kg and 5.0 kg of PCM in the SS. The authors decided

to use smaller bags in the case of tests with 1.0 kg of PCM to better allocate the PCM on the surface of the absorber and to increase the heat transfer surface area between the water and PCM.

2.2. Measuring Devices

Resistance temperature detectors (RTDs) Pt1000 were used to measure the temperatures of PCM (2 RTDs) and fluids, i.e., water (7 RTDs), humid air in the SS (2 RTDs), ambient air (1 RTD), feedwater (1 RTD), and distilled water (1 RTD). Four Pt100 RTD were used to measure the temperature of surfaces, i.e., absorber (2 RTDs), inner glass-cover (1 RTD), and outer glass-cover (1 RTD). The locations of the temperature sensors are shown in Figure 2a, while the top view and 3-D view of the experimental setup are shown in Figure 2b,c, respectively. The float liquid-level-sensor was used to measure the volume of the distilled water, and a pump was used to pump the distillate tank if the condensate volume exceeded 2035 mL. The power of the electric heaters was measured by a wattmeter and controlled by using an electric power-controller. The data from all measuring devices were saved every 1 s on the personal computer. The range and measuring uncertainties of the measuring devices are shown in Table 1.

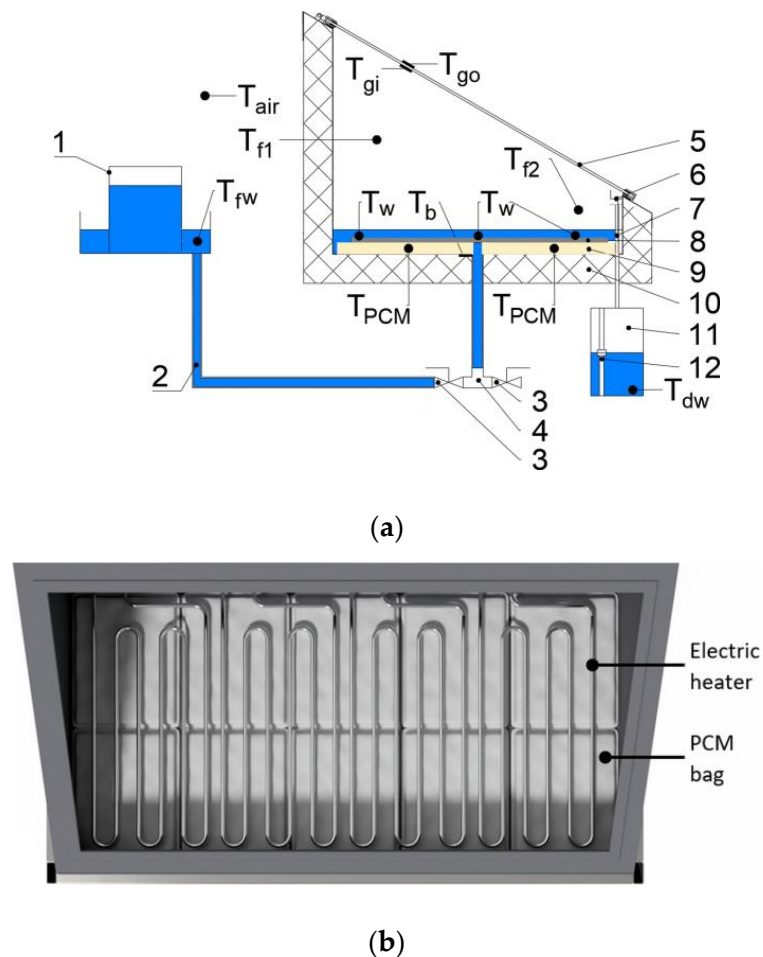


Figure 2. Cont.



(c)

Figure 2. (a) Diagram of the solar still with the locations of the temperature sensors; (b) top view of the solar still; (c) 3-D model of the solar still. 1—feedwater tank; 2—pipe system; 3—shut-off valve; 4—three-way valve; 5—glass cover; 6—distillate trough; 7—distillate channel; 8—electric heater; 9—PCM; 10—thermal insulation; 11—distillate tank; 12—water level sensor; T—temperature. Subscripts: air—ambient air; b—absorber; dw—distilled water; f1, f2—humid air; fw—feedwater; gi—inner glass cover; go—outer glass cover; PCM—phase-change material; w—water.

Table 1. Technical parameters of the measuring devices.

Parameter	Device	Range	Uncertainty
Temperature of fluid	RTD Pt1000	0 to +150 °C	±0.3 °C
Temperature of surface	RTD Pt100	−30 to +200 °C	±(0.1 °C + 0.1%· T) °C
Electric power	Wattmeter	0 to 2880 W	±0.5%
Volume of distilled water	Float liquid-level-sensor	0 to 2365 mL	±30 mL

As mentioned at the beginning of this section, the temperatures of the water, absorber, PCM, and humid air (air–water–vapor mixture in the SS) were measured in two or more locations. Thus, throughout this paper, the temperature of the water, absorber, PCM, and humid air will stand for the average temperature of the respective elements.

2.3. Experimental Procedure

The experiments were conducted to investigate the effects of type and mass of PCM on the performance of the passive single-slope SS. All experiments were conducted under laboratory conditions, to limit the influence of the variability of weather conditions on the results. Thus, the electric heaters, the power of which changed every hour as shown in Figure 3, were used to simulate solar irradiance. The heaters' power was set based on the solar-irradiance data for the typical meteorological year for Kraków [36]. The incident solar irradiance on a 30° sloped surface with an azimuth angle of 0° from May 23 was

chosen. The selected solar irradiance was converted from watts per square meter to watts according to the area of the absorber, and was then implemented into the electric power-controller without any further modifications. The SS was thoroughly cleaned before each experiment, and 10 kg of water was poured into the SS. Then, in the case of SS without PCM, the cover was closed, and the experiment started. In the case of SS with PCM, the appropriate number of PCM bags were placed in the SS, and then the cover was closed, and the experiment started. The experiments were conducted for two different PCM and three different masses of PCM, i.e., 1.0, 2.5, and 5.0 kg. Each experiment lasted 24 h, and additionally, each experiment was repeated twice to check the repeatability of the results. Thus, two experiments without PCM and twelve with PCM were carried out, as presented in Table 2.

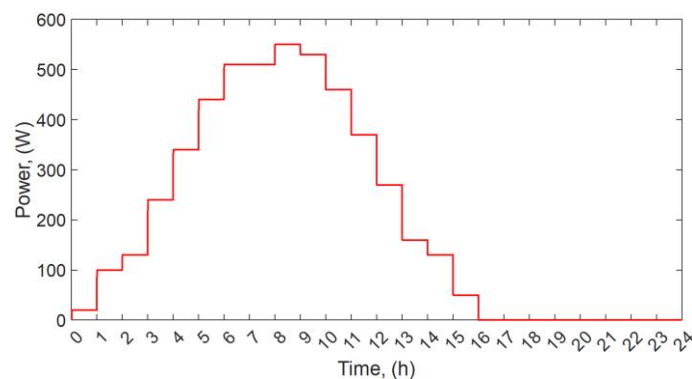


Figure 3. Electric-heater power as a function of time.

Table 2. Experimental conditions.

Experiment	Type of PCM	Mass of PCM, (kg)	PCM-to-Water Mass Ratio, (-)	Type of PCM Bag
1	-	0	0	-
2	-	0	0	-
3	PCM 1	1.0	0.10	Type 2
4	PCM 1	1.0	0.10	Type 2
5	PCM 1	2.5	0.25	Type 1
6	PCM 1	2.5	0.25	Type 1
7	PCM 1	5.0	0.50	Type 1
8	PCM 1	5.0	0.50	Type 1
9	PCM 2	1.0	0.10	Type 2
10	PCM 2	1.0	0.10	Type 2
11	PCM 2	2.5	0.25	Type 1
12	PCM 2	2.5	0.25	Type 1
13	PCM 2	5.0	0.50	Type 1
14	PCM 2	5.0	0.50	Type 1

2.4. PCM Characterization

Two different paraffin waxes were used as PCM during the experiments. Their phase-change temperatures and the latent heat of fusion were determined using DSC (DSC1 from Mettler-Toledo International Inc., Switzerland). The specific heat capacity of the PCM was investigated using temperature modulated TOPEM DSC (DSC1 from Mettler-Toledo International Inc., Zurich, Switzerland). The DSC measurements were carried out with a heating rate of 5 °C/min from −50 °C to 100 °C in a nitrogen atmosphere (30 mL/min) in closed and pierced aluminium pans. The TOPEM DSC measurements were conducted with a heating rate of 2 °C/min, from 0 °C to 100 °C, switching time of 15–36 s, and amplitude of 1 K. The mass of PCM 1 and PCM 2 samples was 5.0 mg and 5.5 mg, respectively.

The thermal conductivity of the PCM was measured at the *Wydziałowe Laboratorium Badań Termofizycznych Wydziału IMIC AGH* (Laboratory of Thermophysical Research at the Faculty of Materials Science and Ceramics at the AGH UST). The thermal conductivity was measured via the transient-line-heat source method using Isomet 2114 (Applied Precision Ltd., Bratislava, Slovakia) with a measurement uncertainty of 5% of reading

+0.001 W/(m·K). The measurements of thermal conductivity were carried out with a needle probe, type IPN 1100, at the temperature of 25 °C.

2.5. Simulations Procedure

After validating the mathematical model, the SS performance was investigated by carrying out simulations. Four series of simulations were conducted, and the simulations were aimed to identify conditions at which the PCM can improve the productivity of the SS. In the first series of simulations, referred to as Case 1, it was assumed that the initial temperatures of the absorber, water, cover, and PCM were equal to the initial temperature of the ambient air. In Case 2, the initial temperature of the water and PCM was assumed to be 50 °C, while the initial temperature of the absorber and glass cover was 15 °C. In Case 3, the initial temperature of each component of the SS was 15 °C. However, in contrast to Cases 1 and 2, the PCM was heated to 63 °C (maximum temperature of the water) outside of the SS, and placed inside the SS after 6.5 h, when the power of the heaters and ambient air-temperature began to decrease. In the last case, i.e., Case 4, it was assumed that the initial temperature of the absorber, water, cover, and PCM was 25 °C and that the bottom and side walls of the SS were not insulated. For all cases, the power of the electric heaters (simulating solar irradiance) and the temperature of the ambient air was set as shown in Figure 4. The mass of PCM varied from 1.0 to 10.0 kg, and its latent heat of fusion, melting onset and endset temperatures, specific heat capacity, and thermal conductivity were assumed to be 190 J/g, 58.5 °C and 61.5 °C, 2.3 J/(g·K), and 0.25 W/(m·K), respectively.

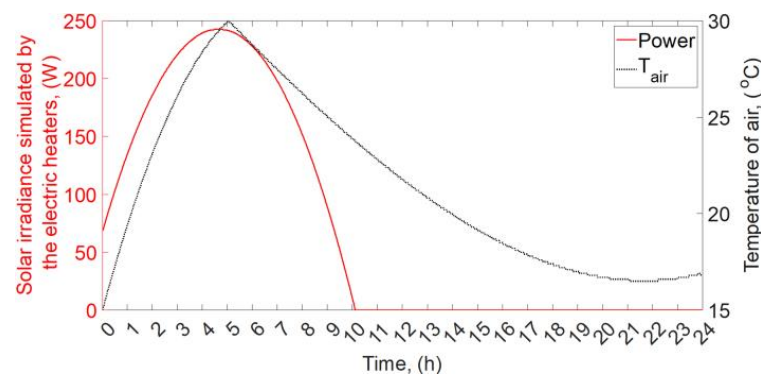


Figure 4. Power of the electric heaters (simulating solar irradiance) and temperature of air for simulations.

In order to compare the performance of the SS, three performance indicators were used: the water temperature, T_w , the temperature difference between water and glass cover, ΔT , and the cumulative productivity, V . The cumulative productivity is the total amount of the distilled water produced in the SS over time. The cumulative productivity in 24 h is referred as to the daily productivity.

3. Mathematical Modeling

A mathematical model of the SS was established, to predict the performance of the SS without and with PCM. Thus, the energy-balance equations for the absorber, water, inner and outer glass-cover, as well as PCM in the case of SS with PCM, were created and solved using MATLAB software, version 9.8 (R2020a, the MathWorks, Inc., Natick, MA, USA). The mathematical model based on the energy-balance equations for individual elements of the SS is a commonly used method of modeling for this type of system, and has been used by numerous researchers [37–39]. To simplify the model, the following assumptions were made [34]:

- There was no temperature gradient in the water;
- The mass of water was constant, as the feedwater tank supplied the freshwater to the SS;

- The thermophysical properties of water and humid air were variable in the function of temperature, while the thermophysical properties of the absorber and glass cover were assumed to be constant;
- The specific heat capacity of the insulating material was neglected;
- Heat conduction from the absorber to the side walls above the free surface of the water was neglected;
- The SS was assumed to be a lumped system, and worked in quasi-steady-state conditions with a 60 s time step, Δt ;
- The glass cover was divided into two parts, inner and outer, with equal masses, and the temperature gradient between them was taken into account;
- The water and inner-glass-cover surfaces were assumed to be parallel and the view factors between them were assumed to be 1;
- The humid air in the SS did not affect or participate in the radiation heat transfer;
- The relative humidity of the humid air in the SS was 100%, and its total pressure, p_t , was 101,300 Pa;
- There was no temperature gradient and no natural convection in the PCM;
- The density and thermal conductivity of the PCM were assumed to be constant.

3.1. Solar Still without PCM

The energy-balance equations for the components, i.e., the absorber, water, inner, and outer glass-cover of the SS without PCM, can be written as [34]:

- Absorber:

$$m_b \cdot c_{pb} \cdot \frac{dT_b}{dt} = a_{h-b} \cdot Q_h - A_b \cdot h_{b-air} \cdot (T_b - T_{air}) - A_w \cdot h_{c,b-w} \cdot (T_b - T_w) \quad (1)$$

- Water:

$$m_w \cdot c_{pw} \cdot \frac{dT_w}{dt} = A_w \cdot h_{c,b-w} \cdot (T_b - T_w) + (1 - a_{h-b}) \cdot Q_h - A_w \cdot h_{r,w-gi} \cdot (T_w - T_{gi}) - A_w \cdot h_{c,w-gi} \cdot (T_w - T_{gi}) - \dot{m}_{w-gi} \cdot r_w - \dot{m}_{w,loss} \cdot r_w \quad (2)$$

- Inner glass-cover:

$$m_{gi} \cdot c_{pg} \cdot \frac{dT_{gi}}{dt} = A_w \cdot h_{r,w-gi} \cdot (T_w - T_{gi}) + A_w \cdot h_{c,w-gi} \cdot (T_w - T_{gi}) + \dot{m}_{w-gi} \cdot r_w - \frac{\lambda_g}{e_g} \cdot A_g \cdot (T_{gi} - T_{go}) \quad (3)$$

- Outer glass cover:

$$m_{go} \cdot c_{pg} \cdot \frac{dT_{go}}{dt} = \frac{\lambda_g}{e_g} \cdot A_g \cdot (T_{gi} - T_{go}) - A_g \cdot h_{r,go-sky} \cdot (T_{go} - T_{sky}) - A_g \cdot h_{c,go-air} \cdot (T_{go} - T_{air}) \quad (4)$$

where a , A , c_p , e , h , m , \dot{m} , Q , r , t , T , and λ are the ratio coefficient, surface area (m^2), specific heat capacity ($J/(kg \cdot K)$), thickness (m), heat transfer coefficient ($W/(m^2 \cdot K)$), mass (kg), mass flow rate (kg/s), heat transfer rate (W), heat of vaporization (J/kg), time (s), temperature ($^{\circ}C$), and thermal conductivity ($W/(m \cdot K)$), respectively. The subscripts *air*, *b*, *c*, *g*, *gi*, *go*, *h*, *loss*, *r*, *sky*, and *w* stand for ambient air, absorber, convective, glass cover, inner glass-cover, outer glass-cover, electric heater, loss to ambient, radiative, sky, and water, respectively. The heat transfer rate from the electric heaters, Q_h , changed every hour, as shown in Figure 3, while the temperature of sky, T_{sky} , was assumed to be equal to the T_{air} because the experiments were conducted under laboratory conditions. The heat transfer coefficients were calculated as [40–44]:

$$h_{b-air} = \left[\frac{e_{ins}}{\lambda_{ins}} + \frac{1}{5.7 + 3.8 \cdot v} \right]^{-1} \quad (5)$$

$$h_{c,b-w} = \frac{Nu_w \cdot \lambda_w}{L_{c,b-w}} \quad (6)$$

$$h_{r,w-gi} = \frac{1}{\frac{1}{\varepsilon_w} + \frac{1}{\varepsilon_g} - 1} \cdot \sigma \cdot \left[(T_w + 273)^2 + (T_{gi} + 273)^2 \right] \cdot (T_w + T_{gi} + 546) \quad (7)$$

$$h_{c,w-gi} = \begin{cases} 1 \cdot Ra_f^{0.25} \cdot \left(\frac{\lambda_f}{L_{c,w-gi}} \right) & \text{for } Gr_f < 2.5 \cdot 10^3 \\ 0.07477 \cdot Ra_f^{0.36} \cdot \left(\frac{\lambda_f}{L_{c,w-gi}} \right) & \text{for } 2.5 \cdot 10^3 \leq Gr_f < 1 \cdot 10^4 \\ 0.21 \cdot Ra_f^{0.25} \cdot \left(\frac{\lambda_f}{L_{c,w-gi}} \right) & \text{for } 1 \cdot 10^4 \leq Gr_f < 3.25 \cdot 10^5 \\ 0.04836 \cdot Ra_f^{0.37} \cdot \left(\frac{\lambda_f}{L_{c,w-gi}} \right) & \text{for } 3.25 \cdot 10^5 \leq Gr_f \end{cases} \quad (8)$$

$$h_{r,go-sky} = \varepsilon_g \cdot \sigma \cdot \left[(T_{go} + 273)^2 + (T_{sky} + 273)^2 \right] \cdot (T_{go} + T_{sky} + 546) \quad (9)$$

$$h_{c,go-air} = \begin{cases} 9.482 \cdot \frac{(T_{go} - T_{air})^{\frac{1}{3}}}{7.238 - |\cos\theta|} & \text{for } T_{go} > T_{air} \\ 1.810 \cdot \frac{(T_{air} - T_{go})^{\frac{1}{3}}}{1.382 + |\cos\theta|} & \text{for } T_{go} < T_{air} \end{cases} \quad (10)$$

where Gr , L_c , Nu , Ra , v , ε , and θ are the Grashof number, characteristic length (m), Nusselt number, Rayleigh number, wind velocity (m/s), emissivity, and inclination angle of the cover ($^\circ$), respectively. The subscripts *ins* and *f* stand for insulation and humid air (air-water-vapor mixture in the SS), respectively. The Nusselt number for the water, Nu_w , was calculated as follows [41,42]:

$$Nu_w = \begin{cases} 0.54 \cdot Ra_w^{0.25} & \text{for } T_b > T_w \text{ and } Ra_w < 10^7 \\ 0.15 \cdot Ra_w^{0.33} & \text{for } T_b > T_w \text{ and } Ra_w \geq 10^7 \\ 0.27 \cdot Ra_w^{0.25} & \text{for } T_b < T_w \end{cases} \quad (11)$$

where the Rayleigh number for water Ra_w is:

$$Ra_w = Gr_w \cdot Pr_w = \frac{g \cdot \beta_w \cdot L_{c,b-w}^3 \cdot \rho_w^2 \cdot (T_b - T_w)}{\mu_w^2} \cdot Pr_w \quad (12)$$

where g , Pr , β , μ , and ρ are the gravitational acceleration (m/s^2), Prandtl number, coefficient of thermal expansion ($1/K$), dynamic viscosity ($Pa \cdot s$), and density (kg/m^3), respectively. The thermophysical properties of water were taken from [45]. The Rayleigh number, Ra_f , for the humid air in the SS (Equation (8)) was calculated as [41,42]:

$$Ra_f = Gr_f \cdot Pr_f = \frac{L_{c,w-gi}^3 \cdot g \cdot (\rho_{f,T_{gi}} - \rho_{f,T_w}) \cdot \rho_f}{\mu_f^2} \cdot \frac{\mu_f \cdot c_{pf}}{\lambda_f} \quad (13)$$

The properties of the humid air were calculated from the correlations given by Tsiligris [46,47].

The total evaporation rate of the water in the SS is calculated using the Dunkle model in the majority of papers published in the open literature. However, in this work, the Chilton–Colburn analogy was used to calculate the evaporation rate of water, and it was assumed that the water vapor is an ideal gas [41]:

$$\dot{m}_w = \frac{h_{c,w-gi}}{\rho_f \cdot c_{pf} \cdot \left(\frac{\lambda_f}{\rho_f \cdot c_{pf} \cdot D_{wa}} \right)^{\frac{2}{3}}} \cdot A_w \cdot \frac{M_w}{R} \left(\frac{p_w}{T_w + 273} - \frac{p_{gi}}{T_{gi} + 273} \right) \quad (14)$$

where D_{wa} , M_w , p , and R are the binary diffusion coefficient of water vapor in air (m^2/s), molar mass of water vapor (kg/mol), partial water-vapor-pressure (Pa), and universal gas

constant (J/(mol·K)), respectively. The D_{wa} , p_w , and p_{gi} can be calculated as presented in Equations (15), (16), and (17), respectively [40,41]:

$$D_{wa} = 1.87 \cdot 10^{-10} \cdot \frac{(T_f + 273)^{2.072}}{p_t / 101325} \quad (15)$$

$$p_w = \exp \left[25.317 - \left(\frac{5144}{T_w + 273} \right) \right] \quad (16)$$

$$p_{gi} = \exp \left[25.317 - \left(\frac{5144}{T_{gi} + 273} \right) \right] \quad (17)$$

However, the mass flow rate of water vapor condensed on the cover, \dot{m}_{w-gi} , is less than the total evaporation rate, \dot{m}_w , due to the following reasons:

- Water vapor condenses partially on the side walls of the SS;
- Some of the water droplets do not flow down the cover;
- Slight vapor-leakage from the SS can occur;
- Some of the water vapor is used to raise and maintain the 100% relative humidity inside the SS.

Therefore, \dot{m}_{w-gi} and $\dot{m}_{w,loss}$ were assumed to be 75% and 25% of the \dot{m}_w , respectively.

In the field of solar stills, the most widely used model for calculating the convective and evaporative heat-transfer-coefficients, and thus the productivity of the SS, is the Dunkle model. However, that model has some limitations, which include [40]:

- The characteristic length between water and cover is not taken into account;
- The equivalent temperature difference between water and cover is 17 °C;
- The thermophysical properties of humid air are calculated for the water at the temperature of 50 °C.

Therefore, in this paper, another relationship (see Equations (8) and (13)) was used to calculate the convective heat-transfer-coefficient. In addition, the Chilton–Colburn analogy was used to calculate the evaporation rate of water. This allowed the above-mentioned limitations of the Dunkle model to be overcome.

3.2. Solar Still with PCM

The energy-balance equations for the absorber, water, inner and outer glass-cover, and PCM can be written as follows:

- Absorber:

$$m_b \cdot c_{pb} \cdot \frac{dT_b}{dt} = A_{b-w} \cdot h_{c,b-w} \cdot (T_w - T_b) + \frac{\lambda_{PCM}}{e_{PCM}} \cdot A_{b-PCM} \cdot (T_{PCM} - T_b) - A_b \cdot h_{b-air} \cdot (T_b - T_{air}) \quad (18)$$

- Water:

$$m_w \cdot c_{pw}(T_w) \cdot \frac{dT_w}{dt} = Q_h - A_w \cdot h_{r,w-gi} \cdot (T_w - T_{gi}) - A_w \cdot h_{c,w-gi} \cdot (T_w - T_{gi}) - \dot{m}_{w-gi} \cdot r_w - \dot{m}_{w,loss} \cdot r_w - A_{b-w} \cdot h_{c,b-w} \cdot (T_w - T_b) - A_{w-PCM} \cdot h_{c,w-PCM} \cdot (T_w - T_{PCM}) \quad (19)$$

- Inner glass-cover:

$$m_{gi} \cdot c_{pg} \cdot \frac{dT_{gi}}{dt} = A_w \cdot h_{r,w-gi} \cdot (T_w - T_{gi}) + A_w \cdot h_{c,w-gi} \cdot (T_w - T_{gi}) + \dot{m}_{w-gi} \cdot r_w - \frac{\lambda_g}{e_g} \cdot A_g \cdot (T_{gi} - T_{go}) \quad (20)$$

- Outer glass-cover:

$$m_{go} \cdot c_{pg} \cdot \frac{dT_{go}}{dt} = \frac{\lambda_g}{e_g} \cdot A_g \cdot (T_{gi} - T_{go}) - A_g \cdot h_{r,go-sky} \cdot (T_{go} - T_{sky}) - A_g \cdot h_{c,go-air} \cdot (T_{go} - T_{air}) \tag{21}$$

- PCM:

$$m_{PCM} \cdot c_{PCM} \cdot \frac{dT_{PCM}}{dt} = A_{w-PCM} \cdot h_{c,w-PCM} \cdot (T_w - T_{PCM}) - \frac{\lambda_{PCM}}{e_{PCM}} \cdot A_{b-PCM} \cdot (T_{PCM} - T_b) \tag{22}$$

where c_{PCM} is the effective heat capacity of the PCM, and can be calculated as [48]:

$$c_{PCM} = \begin{cases} c_s(T_{PCM}) & \text{for } T_{PCM} \leq T_{onset} \\ \frac{c_{s,avg} + c_{l,avg}}{2} + \frac{L}{T_{endset} - T_{onset}} & \text{for } T_{onset} < T_{PCM} < T_{endset} \\ c_l(T_{PCM}) & \text{for } T_{PCM} \geq T_{endset} \end{cases} \tag{23}$$

Subscripts *avg*, *endset*, *l*, *onset*, and *s* stand for average, endset, liquid, onset, and solid, respectively, and *L* is the latent heat of fusion (J/kg). Furthermore, the convective heat-transfer-coefficient, $h_{c,w-PCM}$ was calculated similarly to $h_{c,b-w}$ (Equations (6), (11) and (12)), but with the other characteristic length and changing T_b with T_{PCM} .

The productivity V (mL/m²) of the SS in the time step:

$$V = \frac{1000000 \cdot \dot{m}_{w-gi} \cdot \Delta t}{A_w \cdot \rho_w} \tag{24}$$

The equations presented in Sections 3.1 and 3.2 were implemented into the MATLAB software (version 9.8, R2020a) and Equations (1)–(4) and (18)–(22) were solved using the *ode45* function. The calculated temperatures of the absorber, water, inner and outer cover, and PCM were used to calculate the appropriate heat-transfer-coefficients in the next time-step. The measured power of the electric heaters, ambient air temperature, initial temperatures of the absorber, water, inner and outer glass-cover, and PCM were taken as the main input parameters during modeling in MATLAB. The values of the rest of the inputs for the mathematical model are summarized in Table 3. It is worth noting that some of the input parameters depended on the mass of the PCM, and these parameters are summarized in Table 4.

Table 3. Input parameters for the mathematical modeling—independent of the mass of PCM.

Parameter	Value	Parameter	Value
A_g	0.63 m ²	m_w	10 kg
a_{h-b}	0.5	M_w	0.018016 kg/mol
A_w	0.50 m ²	p_t	101,300 Pa
c_{pb}	460 J/(kg·K) [49]	R	8.314 J/(mol·K)
c_{pg}	880 J/(kg·K) [50]	v	0 m/s
e_g	0.004 m	ϵ_g	0.9
e_{ins}	0.05 m	ϵ_w	0.96
e_{PCM}	0.017 m	θ	30°
g	9.81 m/s ²	λ_g	0.937 W/(m·K)
m_{gi}	3.18 kg	λ_{ins}	0.04 W/(m·K)
m_{go}	3.18 kg	σ	5.67×10^{-8} W/(m ² ·K ⁴)

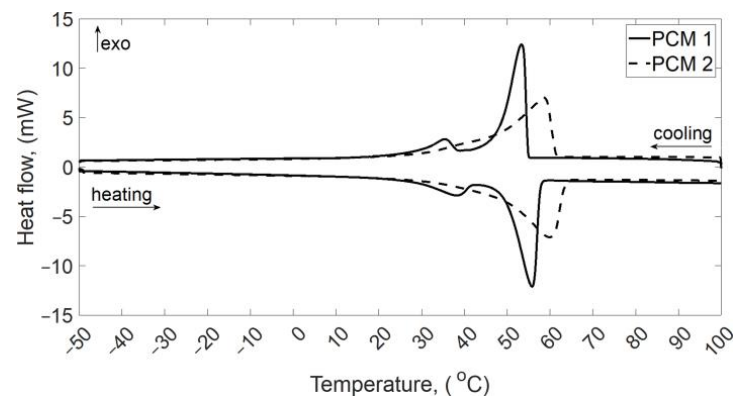
Table 4. Input parameters for the mathematical modeling—dependent on the mass of PCM.

Parameter	Mass of PCM, (kg)			
	0	1.0	2.5	5.0
A_b	0.56 m ²	0.57 m ²	0.58 m ²	0.60 m ²
A_{b-PCM}	-	0.12 m ²	0.21 m ²	0.41 m ²
A_{b-w}	-	0.38 m ²	0.29 m ²	0.09 m ²
A_{w-PCM}	-	0.24 m ²	0.28 m ²	0.55 m ²
m_b	3.45 kg	3.52 kg	3.58 kg	3.71 kg
$L_{c,b-w}$	0.17 m	0.04 m	0.04 m	0.01 m
$L_{c,w-gi}$	0.22 m	0.22 m	0.22 m	0.21 m

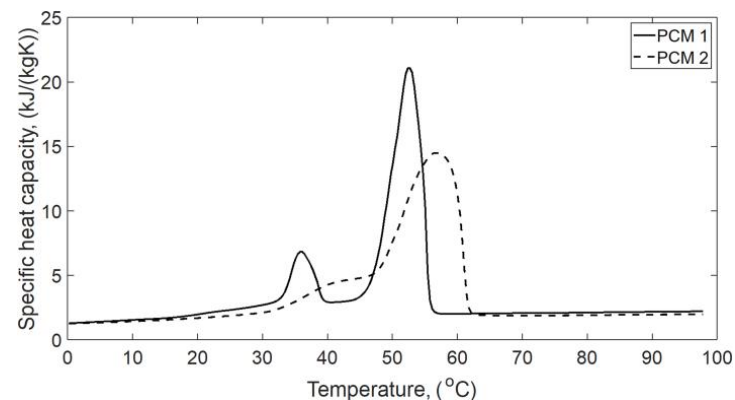
4. Results

4.1. PCM Thermal Properties

The DSC curves and the specific heat capacity of the PCM are presented in Figure 5a,b, respectively. At the DSC curve of PCM 1, two endothermic and two exothermic peaks are visible. The first one, around 38–40 °C, is probably related to the solid–solid phase transition from the orthorhombic phase to the hexagonal phase [51]. The second endothermic peak is related to the melting, while the exothermic peak corresponds to the solidification. Similarly, for PCM 2, the endothermic and exothermic peaks are related to the melting and solidification processes, respectively. The latent heat of fusion of the PCM was calculated by numerical integration of the area under the endothermic peaks. The results of the PCM characterization are summarized in Table 5.



(a)



(b)

Figure 5. (a) DSC curves; (b) specific heat capacity of the PCMs.

Table 5. Thermal properties of the investigated PCMs.

Sample	Melting				Solidification			Solid State	
	T_{onset} (°C)	T_{peak} (°C)	T_{endset} (°C)	L (J/g)	T_{onset} (°C)	T_{peak} (°C)	T_{endset} (°C)	L (J/g)	λ (W/(m·K))
PCM 1	49.3	55.8	57.6	190.7	54.8	53.3	47.7	192.7	0.251
PCM 2	45.8	59.9	63.3	182.7	61.3	58.6	43.6	181.5	0.267

4.2. Model Validation

14 experiments were conducted without PCM and with different types and masses of PCM (see Table 2). The results of the experiments were used to validate the mathematical model presented in Section 3. The authors decided to perform as many as 14 experiments to check the repeatability of the results and verify if the model is applicable for different PCM and variable PCM-to-water mass ratios.

4.2.1. Temperature Changes

Although 14 experiments were conducted, the authors decided to present the water-temperature changes over time only for experiments number 1, 3, 5, 7, 9, 11, and 13. Presenting the results from all of the experiments would make the graphs unreadable, while taking the average from the relevant experiments could distort the results because the SS performance is also affected by the initial temperature of water and temperature of ambient air, which were not the same during each experiment.

Figure 6a–g present the temperature of water and ambient air (T_{air}) over time for the experiments and simulations number 1, 3, 5, 7, 9, 11, and 13. The temperature of ambient air is presented in order to show that the air temperature was different during the experiments, which affected the SS's productivity. Figure 7a–d show a comparison of the water temperature changes depending on the PCM type and mass. As can be seen, the results of the simulations are in reasonably good agreement with the results of the experiments. Furthermore, the root-mean-square error (RMSE) and the maximum deviation (MD) between the simulation and the experiments was calculated for each experiment, to check the correctness of the mathematical model:

$$RMSE = \sqrt{\frac{\sum_{i=1}^N (T_{sim} - T_{exp})^2}{N}} \quad (25)$$

$$MD = \max(T_{sim} - T_{exp}) \quad (26)$$

where N , T_{exp} , and T_{sim} are the number of measurements, temperature obtained in experiments, and temperature obtained in simulations, respectively. The RMSE and MD of the temperatures of the absorber, water, inner glass-cover, outer glass-cover, PCM, and ΔT are summarized in Table 6. As can be seen, the RMSE does not exceed 5.1 °C, which suggests that the model is in good agreement with the experimental results. The MD varies between 1.5 °C and 12.4 °C, which can be considered as a confirmation of the correctness of the mathematical model. Furthermore, no correlations were found between the types of PCM, its mass, and the value of RMSE and MD. Any deviations between the experimental and simulation results may be caused by the assumed simplifications of the mathematical model.

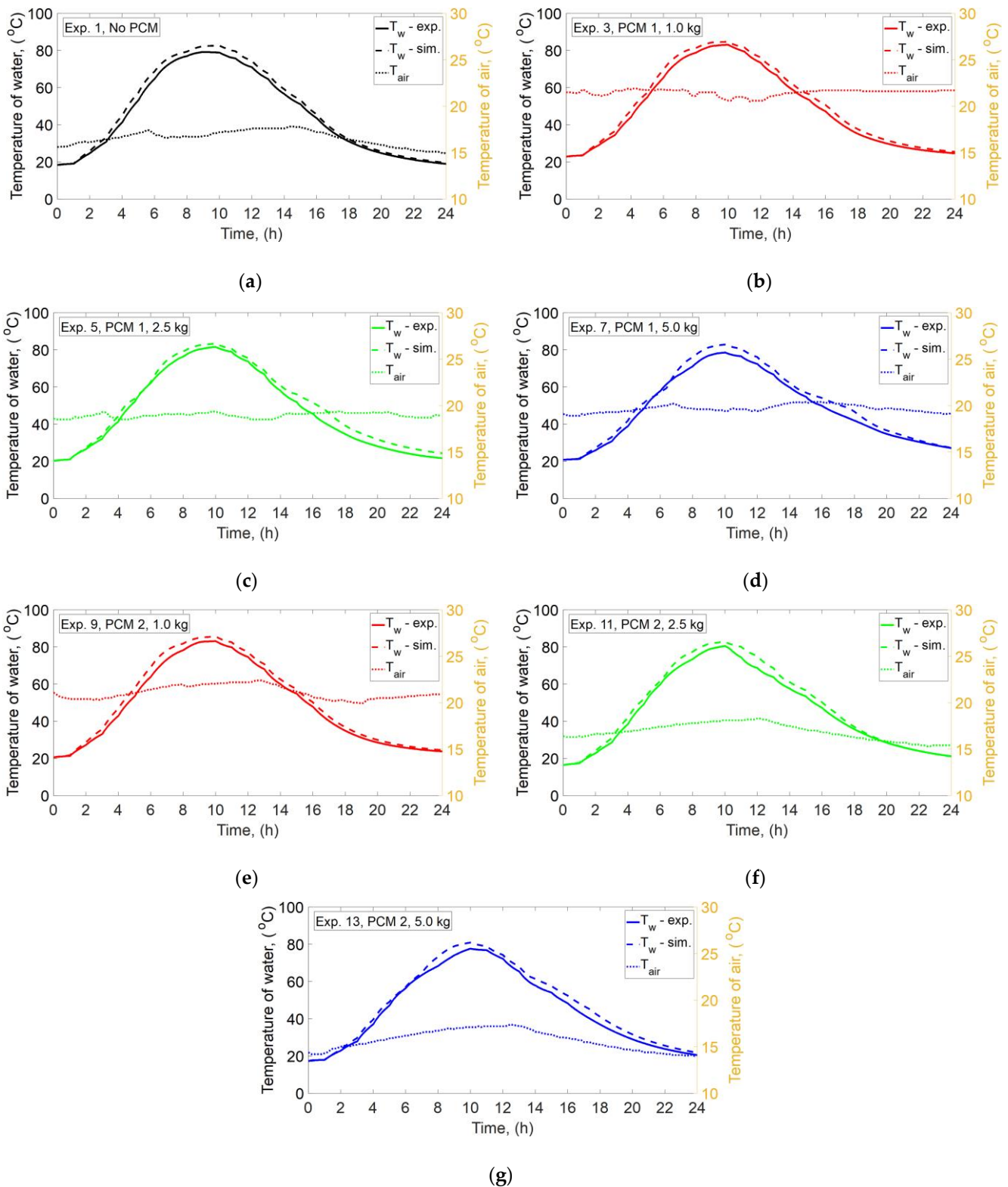


Figure 6. Temperature of ambient air (T_{air}) and temperature of water (T_w) for experiments (exp.) and simulations (sim.): (a) Experiment 1 (no PCM); (b) Experiment 3 (PCM 1, 1.0 kg); (c) Experiment 5 (PCM 1, 2.5 kg); (d) Experiment 7 (PCM 1, 5.0 kg); (e) Experiment 9 (PCM 2, 1.0 kg); (f) Experiment 11 (PCM 2, 2.5 kg); (g) Experiment 13 (PCM 2, 5.0 kg).

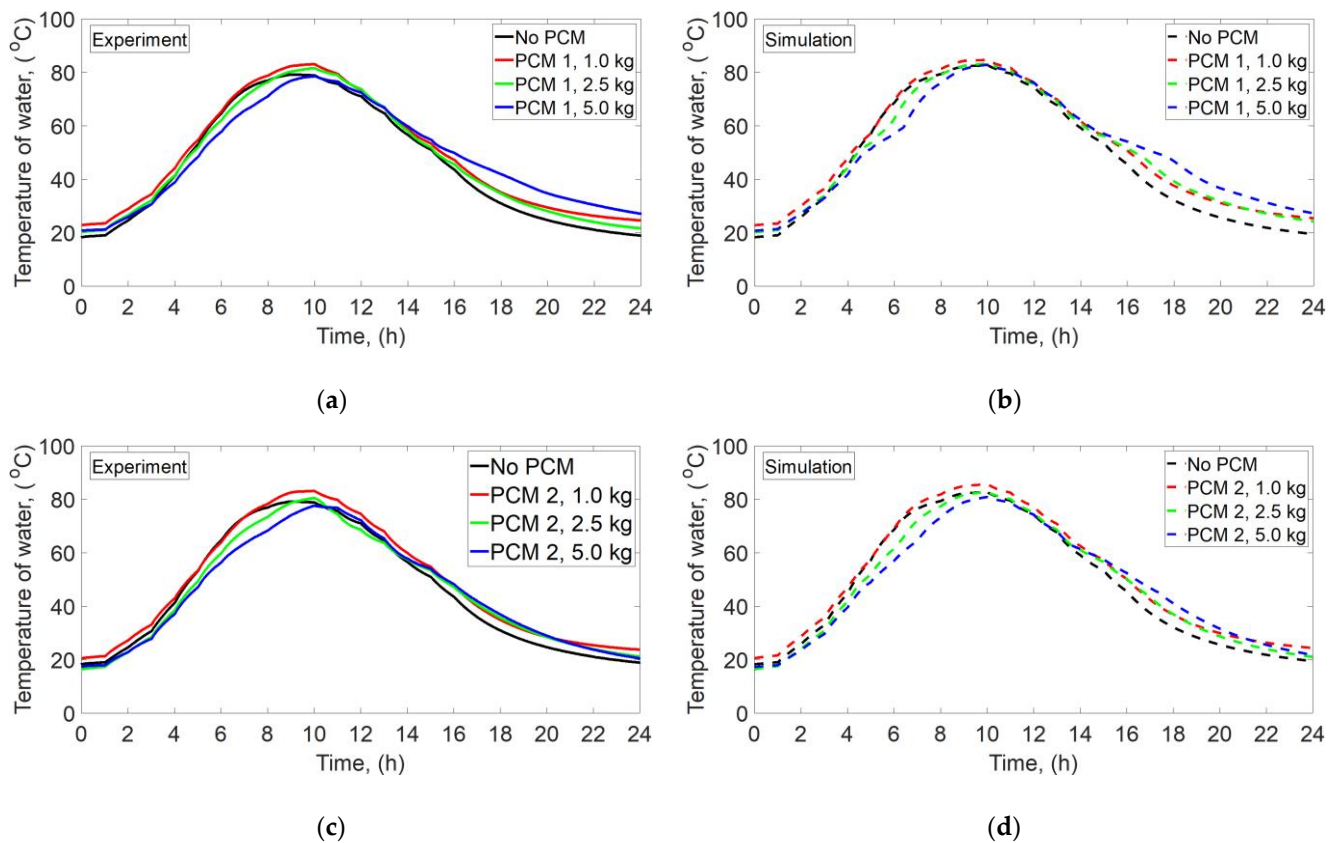


Figure 7. Comparison of water temperature obtained in experiments and simulations: (a) No PCM and PCM 1—experimental results; (b) No PCM and PCM 1—simulation results; (c) No PCM and PCM 2—experimental results; (d) No PCM and PCM 2—simulation results.

Table 6. The root-mean-square error (RMSE) and maximum deviation of temperatures.

Experiment	Root-Mean-Square Error RMSE, (°C)						Maximum Deviation MD, (°C)					
	T_b	T_w	T_{gi}	T_{go}	T_{PCM}	ΔT	T_b	T_w	T_{gi}	T_{go}	T_{PCM}	ΔT
1	3.1	2.5	0.7	2.6	-	2.1	5.7	4.4	2.0	4.9	-	3.6
2	3.4	2.6	1.2	2.9	-	1.9	6.1	4.8	2.6	5.5	-	3.2
3	2.2	2.5	0.9	2.1	2.5	2.4	4.7	4.3	1.5	4.3	5.6	4.3
4	2.6	2.5	0.8	2.5	3.0	2.1	5.5	4.8	2.4	5.1	5.9	3.8
5	4.0	3.2	1.8	2.3	2.2	2.8	12.3	7.3	4.1	5.0	4.5	4.5
6	4.1	2.8	1.2	2.5	2.3	2.3	12.4	6.1	3.5	4.5	4.7	3.9
7	5.1	3.1	1.4	2.7	2.6	2.5	10.6	5.5	3.1	5.0	5.3	4.2
8	4.9	3.1	1.3	2.5	2.5	2.7	9.8	5.6	2.8	4.9	4.7	4.4
9	2.8	2.7	1.3	3.1	3.5	1.8	6.2	5.6	3.8	6.9	8.4	3.7
10	2.6	2.5	0.7	2.6	2.8	2.1	4.9	4.5	1.7	4.8	6.6	3.6
11	4.6	2.9	1.2	2.9	3.1	2.3	11.0	6.6	4.2	7.2	6.8	4.1
12	4.3	2.7	0.9	2.9	3.0	1.9	8.6	5.2	2.7	5.9	6.9	3.2
13	4.7	2.9	1.3	2.5	2.6	2.6	9.5	5.4	2.6	5.4	4.9	4.4
14	4.7	2.6	1.0	2.5	2.4	2.3	9.4	4.7	2.0	5.3	4.8	3.7

As explained in the Introduction, the temperature difference between the water and cover, (ΔT), is one of the main factors affecting the productivity of the SS. The changes in ΔT over time for the experiments and simulations are shown in Figure 8a–d. The results of simulations agree fairly well with the results of the experiments, which is confirmed by a low RMSE and MD (see Table 6).

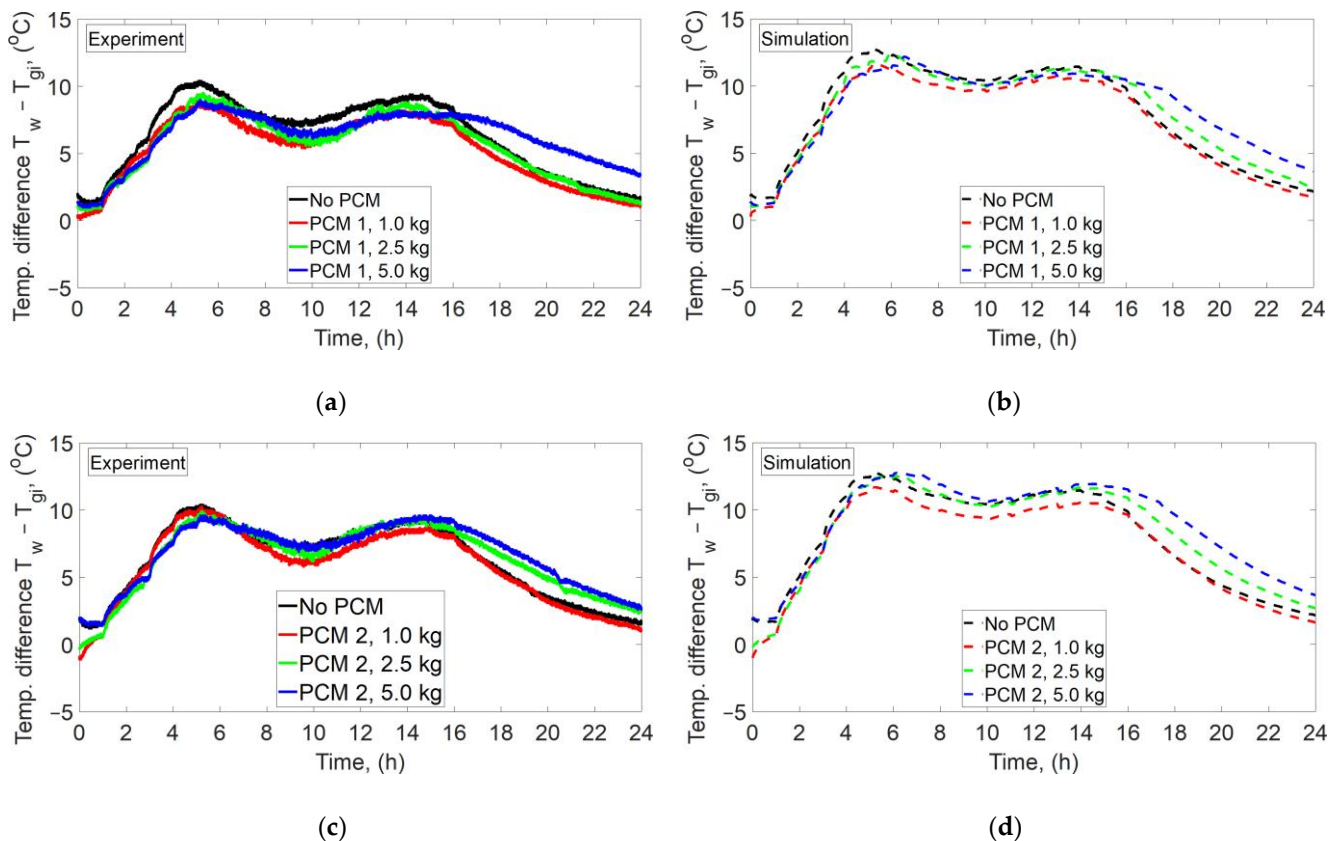


Figure 8. Comparison of the temperature difference between water, (T_w), and inner glass cover, (T_{gi}), obtained in experiments and simulations: (a) No PCM and PCM 1—experimental results; (b) No PCM and PCM 1—simulation results; (c) No PCM and PCM 2—experimental results; (d) No PCM and PCM 2—simulation results.

4.2.2. Productivity

The daily productivity, both experimental and from simulations, of the SS with and without PCM is presented in Figure 9. As can be seen, the daily productivity varies from 8304 to 9116 mL/m²/day, and the PCM did not affect the productivity notably. Such small differences between the results with and without PCM can be attributed to the discrepancies in the operating conditions, i.e., ambient air temperature and initial temperature of the water. Additionally, these results confirm the correctness of the model used for simulations. The maximum percentage difference between the theoretical and experimental productivity is −3.9%. This difference was calculated as:

$$\delta = \frac{V_{sim} - V_{exp}}{V_{exp}} \cdot 100\% \quad (27)$$

where δ , V_{sim} , and V_{exp} are the percentage difference between the results of simulations and experiments, the productivity obtained in simulations, and the productivity obtained in experiments, respectively. The differences between the results of the experiments and theoretical calculations can be attributed to the simplifying assumptions of the model, which are pointed out in Section 3.

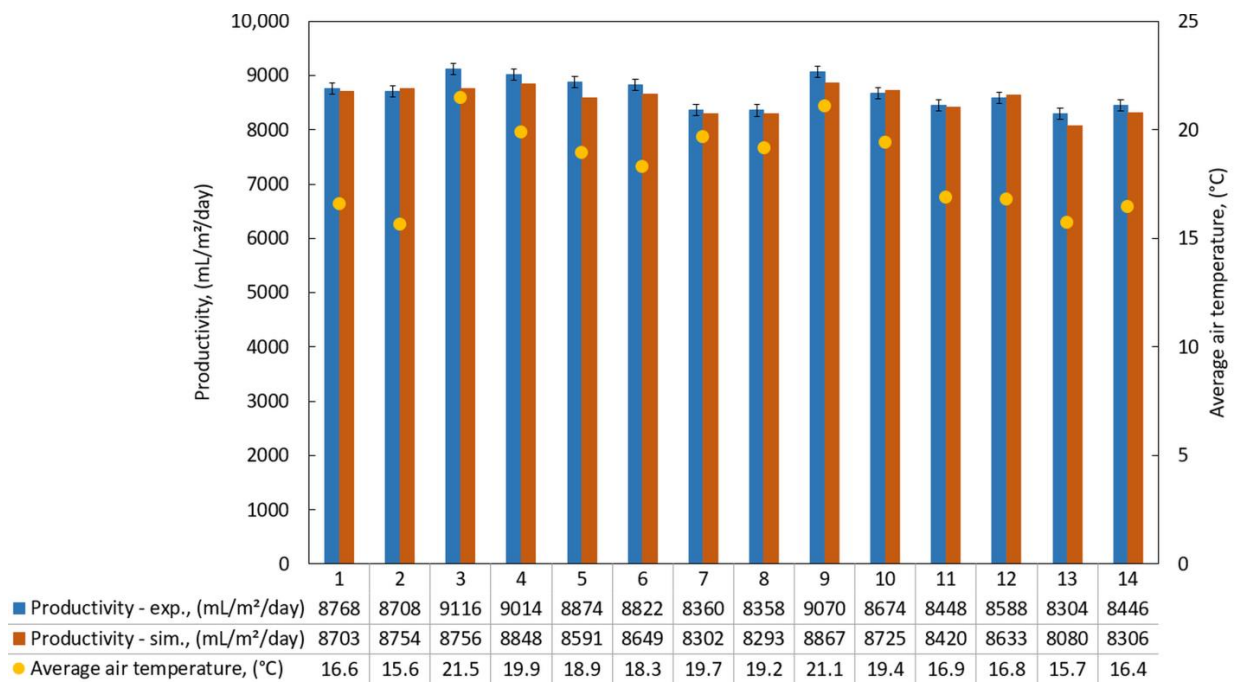


Figure 9. The daily productivity of the SS from experiments (exp.) and simulations (sim.) and the average air temperature. (The numbers 1 through 14 indicate the experimental conditions as given in Table 2).

4.3. Simulation Results

4.3.1. Water-Evaporation Rate

As presented in the Introduction, the productivity of SS depends on the T_w and ΔT , however, the open literature lacks a detailed relationship between the productivity, T_w , and ΔT .

Based on Equation (14), the evaporation rate of water in the SS depends on the convective heat-transfer-coefficient, the partial water-vapor-pressure, and the thermophysical properties of humid air. The above parameters, in turn, depend on the temperature of the water and cover, or in other words, on the temperature of the water, T_w , and the temperature difference between water and cover, ΔT . Thus, the evaporation rate of water in the function of T_w and ΔT can be calculated from the mathematical model presented in Section 3, and the results of these calculations are shown in Figure 10 and Table 7.

Table 7. The evaporation rate of water (mg/s/m²) in the function of the temperature of the water and the temperature difference between water and cover.

ΔT , (°C)	T_w , (°C)														
	20	25	30	35	40	45	50	55	60	65	70	75	80	85	90
1	0.9	1.1	1.5	1.9	2.4	3.1	4.0	5.1	6.6	8.4	10.6	13.4	17.0	21.4	27.1
2	2.2	2.8	3.7	4.8	6.1	7.9	10.1	13.0	16.6	21.1	26.8	33.9	42.9	54.2	68.4
3	3.7	4.8	6.3	8.1	10.4	13.4	17.2	22.1	28.2	35.9	45.6	57.8	73.0	92.2	116.4
4	5.4	7.0	9.1	11.7	15.1	19.4	24.9	31.9	40.8	52.0	66.1	83.7	105.9	133.7	168.7
5	7.1	9.3	12.0	15.5	20.0	25.7	33.0	42.3	54.1	68.9	87.6	111.0	140.4	177.3	223.8
6	8.9	11.6	15.0	19.4	25.0	32.2	41.4	53.1	67.8	86.4	109.9	139.3	176.2	222.5	280.8
7	10.8	14.0	18.1	23.4	30.2	38.9	49.9	64.0	81.8	104.3	132.6	168.1	212.7	268.7	339.1
8	12.6	16.4	21.2	27.4	35.4	45.5	58.5	75.0	95.9	122.3	155.6	197.3	249.7	315.3	398.0
9	14.5	18.8	24.3	31.5	40.6	52.3	67.2	86.1	110.1	140.5	178.6	226.6	286.8	362.3	457.2
10	16.3	21.2	27.4	35.5	45.8	58.9	75.8	97.2	124.3	158.5	201.7	255.9	323.9	409.2	516.4
11	18.1	23.6	30.5	39.5	50.9	65.6	84.3	108.1	138.4	176.5	224.6	285.1	360.8	455.9	575.4
12	19.9	25.9	33.6	43.4	56.0	72.2	92.8	119.0	152.3	194.4	247.4	314.0	397.5	502.3	633.9
13	21.7	28.3	36.6	47.3	61.1	78.7	101.2	129.8	166.1	212.0	269.8	342.5	433.8	548.1	691.8
14	23.5	30.6	39.6	51.2	66.1	85.1	109.4	140.4	179.7	229.4	292.0	370.7	469.5	593.4	748.9
15	25.2	32.8	42.5	55.0	71.0	91.4	117.5	150.8	193.0	246.4	313.8	398.5	504.7	637.9	805.1

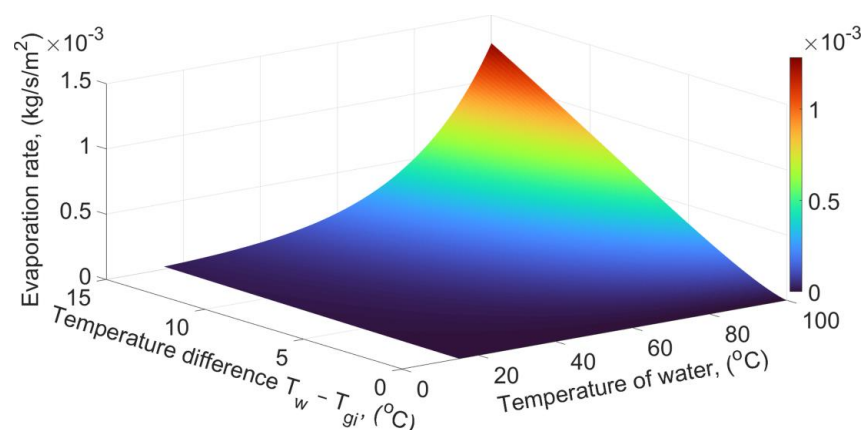


Figure 10. Water-evaporation rate in the function of the water temperature and the temperature difference between water and glass cover.

As can be seen from Figure 10 and Table 7, the evaporation rate of water increases with an increasing T_w and ΔT , which is a confirmation of Tsilingiris' [10] finding. The growth rate of water-evaporation rate is approximately constant with increasing T_w , e.g., when T_w increases from 20 °C to 25 °C, the evaporation rate increases by 22.2%, and when T_w increases from 85 °C to 90 °C, the evaporation rate increases by 26.6%. In contrast, the growth rate of water evaporation decreases with increasing ΔT , e.g., when ΔT increases from 1 °C to 2 °C, the evaporation rate rises by 144.4% but when ΔT increases from 14 °C to 15 °C, the evaporation rate rises by 7.2%. Therefore, from the standpoint of maximizing the productivity of SS, it is more advantageous to run the evaporation at the highest possible T_w , even at the expense of lowering the ΔT .

Knowing the evaporation rate of water as a function of T_w and ΔT , the authors carried out four series of simulations, described in Section 2.5. The results of these simulations are discussed in detail in Section 4.3.2, Section 4.3.3, Section 4.3.4, Section 4.3.5., while the daily productivity in each case is summarized in Table 8.

4.3.2. Results of Case 1

In the first case, it was assumed that the initial temperatures of the absorber, water, cover, and PCM were equal to the initial temperature of the ambient air. The obtained water-temperature changes are presented in Figure 11. In the case of SS with PCM, some energy supplied to the system is used to heat and melt the PCM, and hence the T_w does not increase so much, compared to the case without PCM. As the mass of PCM increases, the maximum water-temperature decreases. However, as the PCM solidifies, it releases and transfers heat to the water, and thus, the T_w remains higher for a longer time. This finding is consistent with the results reported by Yousef and Hassan [21], who concluded that the PCM lowers the maximum water temperature but keeps the water warmer for a longer period.

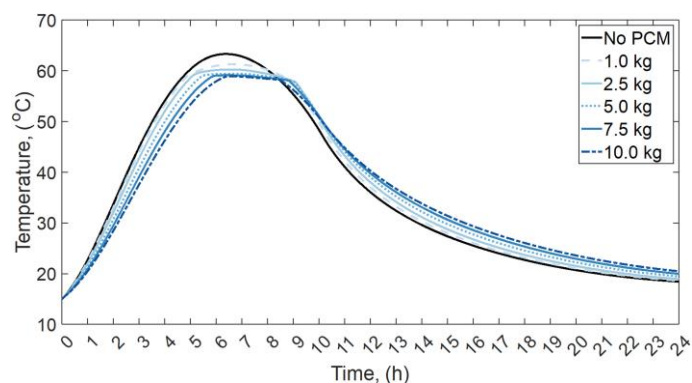


Figure 11. Water temperature in the SS with different masses of PCM—Case 1.

Figure 12 shows the temperature difference between water and cover, ΔT . As can be observed, during the first 8 h, the maximum ΔT was maintained for the SS without PCM, and as the mass of PCM increased, the ΔT decreased. However, by using PCM, a large ΔT was maintained after approximately 8 h, which is when the power of the heaters and the temperature of the ambient air began to decrease.

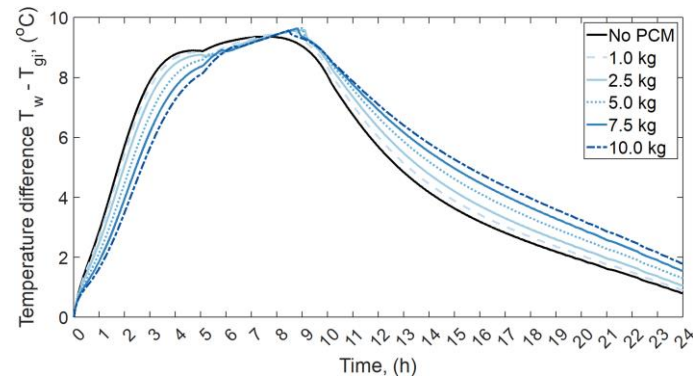


Figure 12. The temperature difference between water and inner glass cover in the SS with different masses of PCM—Case 1.

The large ΔT after 8 h from the beginning, for the SS with PCM, was supposed to improve the productivity. Nevertheless, the improvement did not occur, which is shown in Figure 13. Furthermore, as the mass of PCM increased, productivity decreased. This supports the finding of Mousa and Gujarathi [29], who reported that PCM negatively affects the productivity of SS. Such a result can be attributed to the fact that, as discussed in Section 4.3.1, the evaporation rate of water depends on T_w and ΔT . The maximum T_w for the SS without PCM is approximately 63 °C, and then ΔT is approximately 8–9 °C (see Figures 11 and 12). Consequently, the evaporation rate is then approximately 110–130 mg/s/m². On the other hand, analyzing the SS with, e.g., 5 kg of PCM, the maximum T_w is approximately 57 °C and ΔT is then approximately 9 °C. Therefore, the evaporation rate for the SS with 5 kg of PCM is then approximately 85–95 mg/s/m². Going further, and analyzing the temperatures at, for example, the fifteenth h, it can be seen that the evaporation rate for the SS without PCM, and with 5 kg of PCM, is approximately 6 and 11 mg/s/m², respectively. Therefore, high T_w and ΔT for the SS with PCM after approximately 8 h from the beginning do not compensate for low T_w during the initial stage of the process. Consequently, when the initial temperature of the absorber, water, cover, and PCM is equal to the initial temperature of the ambient air, the PCM negatively affects the productivity of the SS, and the maximum reduction in productivity (10.8%) is obtained for 10.0 kg of PCM, as compared to the SS without PCM.

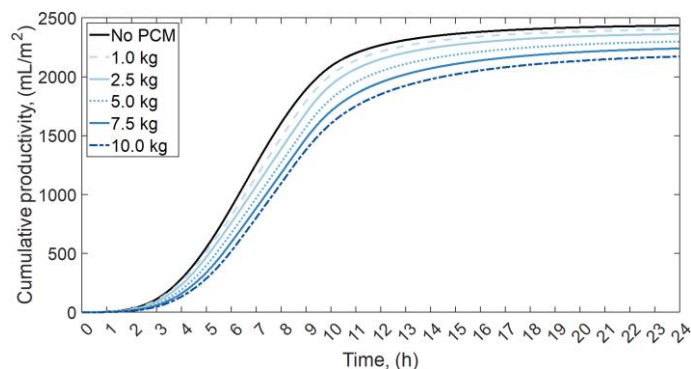


Figure 13. The cumulative productivity of the SS with different masses of PCM—Case 1.

On the other hand, most of the research indicates that the PCM improves the productivity of SS. Thus, the question arises as to what these discrepancies are due to. A plausible explanation of why in some cases PCM improve the performance of SS and in others they do not, is the fact of the design differences, e.g., a lack of thermal insulation at the side walls and the fact that the entire SS is made of other material, e.g., glass [21]. Furthermore, in the majority of papers, the research is conducted under real conditions, often over several consecutive days. For example, SS without PCM is investigated one day, and SS with PCM the next day, as in, for example, the paper in [25]. Consequently, it cannot be excluded that in such cases the improvement of productivity after PCM application is due to more favorable atmospheric conditions, i.e., solar irradiance, ambient air temperature, and wind speed, rather than the PCM itself.

4.3.3. Results of Case 2

In the second case, it was assumed that the initial temperature of the water and PCM was 50 °C, and the initial temperature of the absorber and cover was 15 °C.

The water temperature changes for Case 2 are shown in Figure 14. As can be seen, for the SS without PCM, T_w decreases from 50 °C to approximately 45 °C during the first hour, and then increases to approximately 63 °C. At the same time, the decrease in T_w in the SS with PCM is much lower. After approximately the third hour, the temperature changes are similar to those in Case 1.

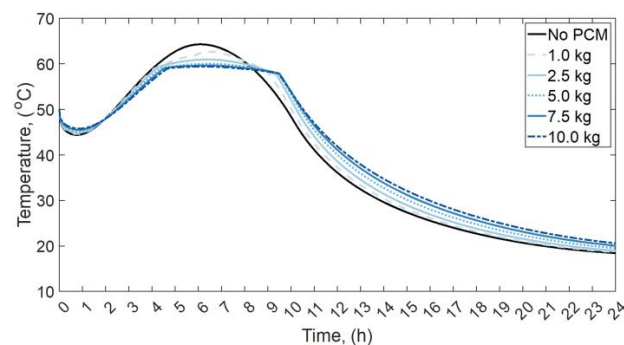


Figure 14. Water temperature in the SS with different masses of PCM—Case 2.

The ΔT changes for Case 2 are presented in Figure 15. A sudden drop of ΔT is reported during the first 15 min. This drop is a result of rapid water-evaporation and condensation on the cover, caused by a large initial T_w and ΔT . Then, the ΔT remains fairly stable, in the range of approximately 9–10 °C, until approximately the eighth h for the SS without PCM and until approximately the ninth h for the SS with 10 kg of PCM. As a result, the productivity of the SS (see Figure 16) with PCM is greater for the first four h and then from approximately the fifteenth h, compared to the SS without PCM. Consequently, the daily productivity of the SS increases, up to 2.4%, with the increasing mass of the PCM (see Table 8).

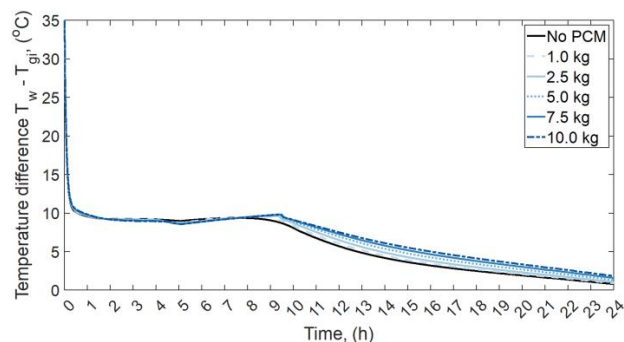


Figure 15. The temperature difference between water and inner glass cover in the SS with different masses of PCM—Case 2.

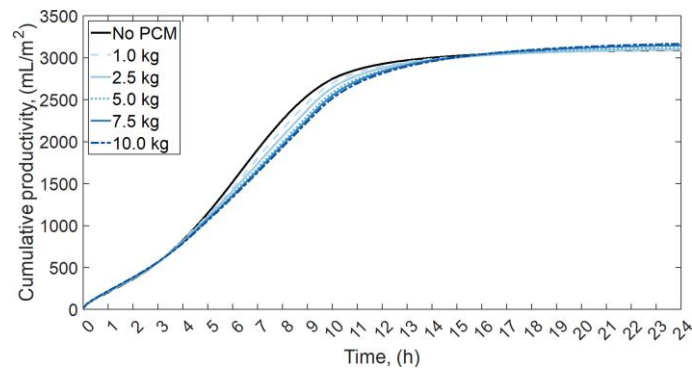


Figure 16. The cumulative productivity of the SS with different masses of PCM—Case 2.

Table 8. The productivity of the SS with and without PCM for different cases.

Case	Mass of PCM, (kg)	Productivity, (mL/m ² /day)	Percentage Improvement (+) or decline (−) *, (%)
1	0	2434	-
1	1.0	2401	−1.4
1	2.5	2363	−2.9
1	5.0	2299	−5.5
1	7.5	2240	−8.0
1	10.0	2172	−10.8
2	0	3093	-
2	1.0	3091	−0.1
2	2.5	3100	+0.2
2	5.0	3118	+0.8
2	7.5	3149	+1.8
2	10.0	3167	+2.4
3	0	2434	-
3	1.0	2559	+5.1
3	2.5	2738	+12.5
3	5.0	3022	+24.2
3	7.5	3300	+35.6
3	10.0	3580	+47.1
4	0	1491	-
4	1.0	1507	+1.1
4	2.5	1492	+0.1
4	5.0	1478	−0.9
4	7.5	1437	−3.6
4	10.0	1396	−6.4

* Compared to the same case but without PCM.

4.3.4. Results of Case 3

In the third case, the initial temperature of each component of the SS was 15 °C. However, as opposed to Cases 1 and 2, the PCM was heated to 63 °C (maximum temperature of the water) outside of the SS, and placed inside the SS after 6.5 h, when the power of the heaters and ambient air temperature began to decrease.

The T_w in the function of time for Case 3 is shown in Figure 17. In Case 3, the entire energy supplied to the SS is used to heat only water and the absorber. After 6.5 h, the temperature of water for the SS without PCM decreases in the same way as in Case 1. However, in the case of SS with PCM, the high T_w and ΔT (see Figure 18) are maintained longer, because PCM releases its heat. Thus, in Case 3, the productivity of the SS with PCM can be improved by up to 47.1%, compared to the SS without PCM, as presented in Figure 19.

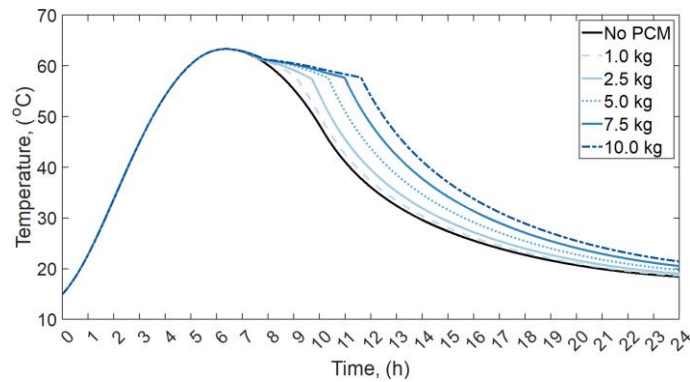


Figure 17. Water temperature in the SS with different masses of PCM—Case 3.

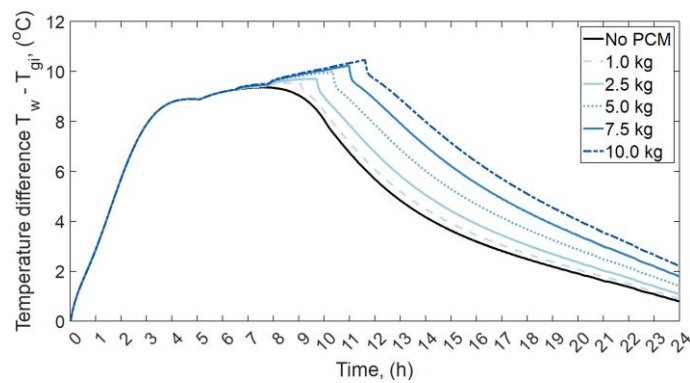


Figure 18. The temperature difference between water and inner glass cover in the SS with different masses of PCM—Case 3.

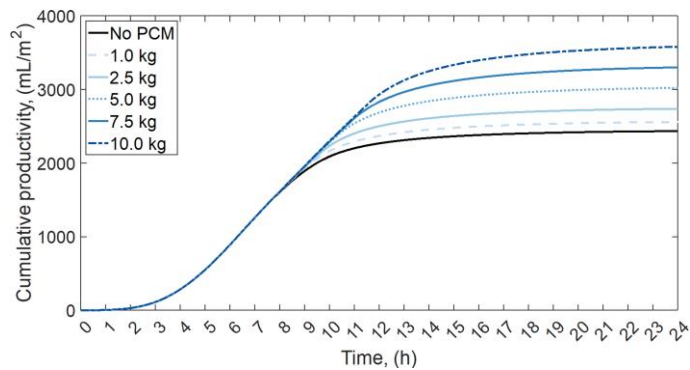


Figure 19. The cumulative productivity of the SS with different masses of PCM—Case 3.

4.3.5. Results of Case 4

The fourth case assumes that the initial temperature of the absorber, water, cover, and PCM was 25 °C, and that the bottom and side walls of the SS were not insulated.

The T_w for Case 4 is shown in Figure 20. When comparing the maximum T_w for Case 1 and Case 4, it can be stated that as the mass of PCM increases, the difference between the maximum T_w for Case 1 and Case 4 decreases. A possible reason for such a phenomenon is that in the absence of thermal insulation of the absorber and side walls, PCM may take over the role of thermal insulation. In addition, as indicated by Khalifa and Hamood [52], the productivity of SS with thermal insulation is greater than that without thermal insulation. Nevertheless, the high mass of PCM causes the T_w , and hence the ΔT (Figure 21), to be lower for the SS with PCM compared to the SS without PCM during the first 7–8 h. As a result, for Case 4, a slight improvement in productivity (Figure 22) after the application of

PCM is obtained only for the SS with 1.0, and 2.5 kg of PCM. The productivity improvement is 1.1% and 0.1% for 1.0 kg, and 2.5 kg of PCM, respectively.

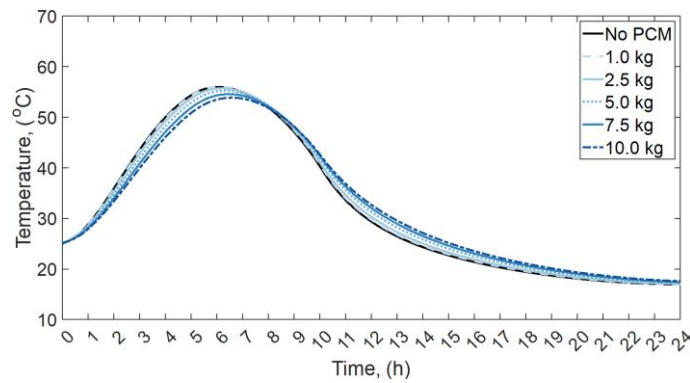


Figure 20. Water temperature in the SS with different masses of PCM—Case 4.

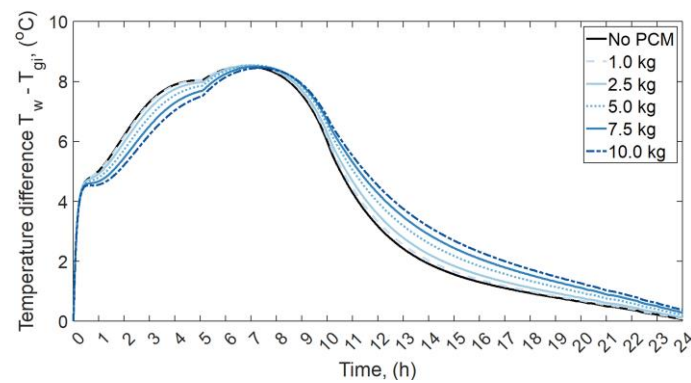


Figure 21. The temperature difference between water and inner glass cover in the SS with different masses of PCM—Case 4.

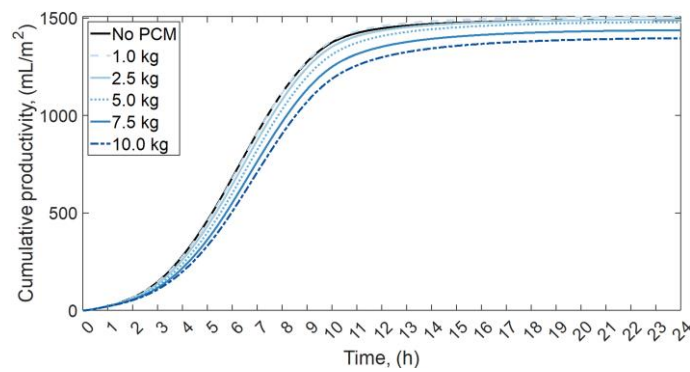


Figure 22. The cumulative productivity of the SS with different masses of PCM—Case 4.

Table 9 summarizes the most important results of this work and of the selected previous papers available in the open literature. Percentage improvement or decline in Table 9 refers to the daily productivity, and was calculated as:

$$P = \frac{V_{withPCM} - V_{withoutPCM}}{V_{withoutPCM}} \cdot 100\% \tag{28}$$

where P is the percentage improvement or decline after PCM application into the SS (%), V is the daily productivity ($\text{mL}/\text{m}^2/\text{day}$), and the subscripts *withPCM* and *withoutPCM* refer to the SS with PCM and without PCM, respectively. Therefore, the P indicator shows the impact of PCM on the performance of SS obtained by individual research teams. For

example, in the case of Yousef and Hassan [21], P is +9.5%, which means that the daily productivity of SS with PCM (paraffin wax) investigated by Yousef and Hassan [21] is 9.5% greater than the productivity of the SS without PCM investigated by Yousef and Hassan [21].

Table 9. Comparison of the results.

Reference	Location	m_{PCM}/m_w	Percentage Improvement (+) or Decline (−) *, (%)	Remark
Yousef and Hassan [21]	Egypt	1.13	+9.5	Paraffin wax
Chaichan and Kazem [22]	Iraq	n.a.	+14.3	Paraffin wax
			+60.5	Paraffin wax + Al ₂ O ₃ (3 wt.%)
Kabeel et al. [23]	Egypt	1.46	+62.6	Paraffin wax
			+94.5	Paraffin wax + graphite nanoparticles (20% mass fraction)
Shalaby et al. [25]	Egypt	0.75 0.51	+12.0	Paraffin wax
Sonker et al. [26]	India	0.23	+70.2	Lauric acid
			+76.8	Stearic acid
			+91.2	Paraffin wax
Mousa et al. [27]	Oman	0.17	+0.5	Tricosane
		0.35	−13.1	
		0.51	−12.3	
Al-Harashsheh et al. [28]	Jordan	0.11	+4.5	Sodium thiosulfate pentahydrate
		0.13	+7.1	
		0.18	+16.8	
		0.25	+15.6	
		0.38	+19.0	
Kateshia and Lakhera [30]	India	0.75	+2.6	Palmitic acid
		1.50	+15.8	
		2.24	+29.0	
Tabrizi et al. [31]	Iran	n.a.	−5.6	Sunny day
			+61.9	Cloudy day Paraffin wax
Sarhaddi et al. [32]	Iran	n.a.	−6.0	Sunny day
			+28.6	Cloudy day
				Paraffin wax
This work—max. increase	Poland	0.1	+4.0	Experiment, max. increase
		0.5	−5.3	Experiment, max. decrease
		1.0	+47.1	Simulation—Case 3, max. increase
		1.0	−10.8	Simulation—Case 1, max. decrease

* Compared to the same case but without PCM.

5. Conclusions

This paper presents the results of the experimental and theoretical investigation of the effects of using PCM on the performance of the passive single-slope solar still. The experimental data were used to validate the mathematical model describing the heat and mass transfer inside the SS. The ordinary differential equations from the model were solved numerically, and the approximate solutions of the temperatures were obtained. Then, through the mathematical modeling, a detailed relationship between the water-evaporation rate, T_w , and ΔT was determined. Furthermore, the influence of the PCM-to-water mass

ratio on the productivity of SS, depending on the operating conditions, was established. These novel findings fill a knowledge gap representing the lack of explanation as to why PCM does not improve the productivity of SS in certain cases.

When the initial temperatures of the absorber, water, cover, and PCM are the same, and they are at least 15 °C lower than the maximum temperature of the water, the productivity of the SS with PCM is lower by up to 10.8%, compared to the SS without PCM. However, when the initial temperatures of the water and PCM are 50 °C, the PCM can improve the productivity of the SS by up to 2.4%. Furthermore, if the PCM were heated up outside of the SS and put into the SS when the temperature of the water starts decreasing, it could improve productivity by up to 47.1%. In the case of a lack of thermal insulation of the SS, the PCM can take over the role of an insulator and improve productivity, by up to 1.1%.

This paper undoubtedly provides a valuable new contribution to the field of solar stills.

Author Contributions: Conceptualization, E.R. and K.S.; methodology, E.R.; software, E.R.; validation, W.K.; formal analysis, Ł.M. and K.S.; investigation, E.R., W.K., Ł.L., K.P., M.S. and P.R.; data curation, E.R.; writing—original draft preparation, E.R.; writing—review and editing, Ł.M., K.S., K.P., M.S. and P.R.; visualization, Ł.L.; supervision, Ł.M.; project administration, Ł.M.; funding acquisition, Ł.M. All authors have read and agreed to the published version of the manuscript.

Funding: This research was funded by the Ministry of Science and Higher Education, Poland, grant AGH number 16.16.210.476.

Data Availability Statement: The data presented in this study are available on request from the corresponding author.

Conflicts of Interest: The authors declare no conflict of interest.

Nomenclature

A_b	absorber surface-area, m ²
A_{b-PCM}	heat-transfer surface-area between absorber and PCM, m ²
A_{b-w}	heat-transfer surface-area between absorber and water, m ²
A_g	glass-cover surface area, m ²
a_{H-b}	ratio of the heat supplied to the absorber to the total power of the electric heaters
A_w	water surface area, m ²
c_l	specific heat capacity of liquid PCM, J/(kg·K)
$c_{l,avg}$	average specific-heat-capacity of liquid PCM, J/(kg·K)
c_{pb}	absorber specific-heat-capacity, J/(kg·K)
c_{PCM}	effective specific-heat-capacity of PCM, J/(kg·K)
c_{pf}	humid air (air–water-vapor mixture) specific heat capacity, J/(kg·K)
c_{pg}	glass specific-heat-capacity, J/(kg·K)
c_{pw}	water specific-heat-capacity, J/(kg·K)
c_s	specific heat capacity of solid PCM, J/(kg·K)
$c_{s,avg}$	average specific-heat-capacity of solid PCM, J/(kg·K)
D_{wa}	binary diffusion coefficient of water vapor in air, m ² /s
e_g	glass-cover thickness, m
e_{ins}	insulation thickness, m
e_{PCM}	PCM thickness, m
g	gravitational acceleration, m/s ²
Gr_f	Grashof number for humid air (air–water-vapor mixture)
Gr_w	Grashof number for water
h_{b-air}	overall heat-transfer-coefficient between absorber and ambient air, W/(m ² ·K)
$h_{c,b-w}$	convective heat-transfer-coefficient between absorber and water, W/(m ² ·K)
$h_{c,go-air}$	convective heat-transfer-coefficient between outer glass cover and ambient air, W/(m ² ·K)
$h_{c,w-gi}$	convective heat-transfer-coefficient between water and inner glass-cover, W/(m ² ·K)
$h_{c,w-PCM}$	convective heat-transfer-coefficient between water and PCM, W/(m ² ·K)
h_{mass}	mass transfer coefficient, m/s
$h_{r,go-sky}$	radiation heat-transfer-coefficient between outer glass-cover and sky, W/(m ² ·K)
$h_{r,w-gi}$	radiation heat-transfer-coefficient between water and inner glass-cover, W/(m ² ·K)

L	latent heat of fusion, J/kg
$L_{c,b-w}$	characteristic length of convective heat transfer between absorber and water, m
$L_{c,w-gi}$	characteristic length of the solar still, m
m_b	mass of the absorber, kg
m_{gi}	mass of the inner glass-cover, kg
m_{go}	mass of the outer glass-cover, kg
m_w	mass of the water, kg
M_w	molar mass of water vapor, kg/mol
\dot{m}_w	total mass-flow-rate of evaporated water, kg/s
$\dot{m}_{w,loss}$	lost mass-flow-rate of condensate, kg/s
\dot{m}_{w-gi}	mass flow rate of condensate on the glass cover, kg/s
N	number of measurements
Nu_w	Nusselt number for water
p_{gi}	partial water-vapor-pressure at the inner glass-cover temperature, Pa
Pr_f	Prandtl number for humid air (air–water-vapor mixture)
Pr_w	Prandtl number for water
p_t	total pressure of humid air (air–water-vapor mixture), Pa
p_w	partial water-vapor-pressure at the water temperature, Pa
Q_h	power of the electric heaters, W
R	universal gas constant, J/(mol·K)
Ra_f	Rayleigh number for humid air (air–water-vapor mixture)
Ra_w	Rayleigh number for water
r_w	latent heat of evaporation, J/kg
t	time, s
T_{air}	ambient air temperature, °C
T_b	absorber temperature, °C
T_{endset}	endset temperature of the PCM phase transition, °C
T_{exp}	temperature obtained in experiments, °C
T_f	humid air temperature, °C
T_{gi}	inner glass-cover temperature, °C
T_{go}	outer glass-cover temperature, °C
T_{onset}	onset temperature of the PCM phase transition, °C
T_{PCM}	PCM temperature, °C
T_{sim}	temperature obtained in simulations, °C
T_{sky}	sky temperature, °C
T_w	water temperature, °C
v	wind speed, m/s
V	productivity, mL/m ²
V_{exp}	daily productivity obtained in experiments, mL/m ² /day
V_{sim}	daily productivity obtained in simulations, mL/m ² /day
β_w	coefficient of thermal expansion of water, 1/K
ΔT	temperature difference between water and glass cover, °C
δ	percentage difference between the results of simulations and experiments, %
ε_g	glass emissivity
ε_w	water emissivity
θ	inclination angle of the glass cover, °
λ_f	thermal conductivity of humid air (air–water-vapor mixture), W/(m·K)
λ_g	thermal conductivity of glass, W/(m·K)
λ_{ins}	thermal conductivity of insulation, W/(m·K)
λ_{PCM}	thermal conductivity of PCM, W/(m·K)
λ_w	thermal conductivity of water, W/(m·K)
μ_f	dynamic viscosity of humid air (air–water-vapor mixture), Pa·s
μ_w	dynamic viscosity of water, Pa·s
ρ_f	density of humid air (air–water-vapor mixture), kg/m ³
$\rho_{f,T_{gi}}$	density of humid air (air–water-vapor mixture) at the inner glass-cover temperature, kg/m ³
ρ_{f,T_w}	density of humid air (air–water-vapor mixture) at the water temperature, kg/m ³
ρ_w	density of water, kg/m ³
σ	Stefan–Boltzmann constant, W/(m ² ·K ⁴)

References

1. World Health Organization. Available online: <https://www.who.int/en/news-room/fact-sheets/detail/drinking-water> (accessed on 20 July 2020).
2. Chakraborty, R.; Khan, K.M.; Dibaba, D.T.; Khan, M.A.; Ahmed, A.; Islam, M.Z. Health Implications of Drinking Water Salinity in Coastal Areas of Bangladesh. *Int. J. Environ. Res. Public Health* **2019**, *16*, 3746. [CrossRef] [PubMed]
3. United States Geological Survey How Much Water Is There on Earth? Available online: https://www.usgs.gov/special-topic/water-science-school/science/how-much-water-there-earth?qt-science_center_objects=0#qt-science_center_objects (accessed on 20 July 2020).
4. Jones, E.; Qadir, M.; van Vliet, M.T.H.; Smakhtin, V.; Kang, S.-M. The state of desalination and brine production: A global outlook. *Sci. Total Environ.* **2019**, *657*, 1343–1356. [CrossRef] [PubMed]
5. Gugulothu, R.; Somanchi, N.S.; Reddy, K.V.K.; Gantha, D. A Review on Solar Water Distillation Using Sensible and Latent Heat. *Procedia Earth Planet. Sci.* **2015**, *11*, 354–360. [CrossRef]
6. Arunkumar, T.; Raj, K.; Chaturvedi, M.; Thenmozhi, A.; Denkenberger, D.; Tingting, G. A review on distillate water quality parameter analysis in solar still. *Int. J. Ambient. Energy* **2021**, *42*, 1335–1342. [CrossRef]
7. Tuly, S.S.; Sarker, M.R.I.; Das, B.K.; Rahman, M.S. Effects of design and operational parameters on the performance of a solar distillation system: A comprehensive review. *Groundw. Sustain. Dev.* **2021**, *14*, 100599. [CrossRef]
8. Omara, Z.M.; Abdullah, A.S.; Kabeel, A.E.; Essa, F.A. The cooling techniques of the solar stills' glass covers—A review. *Renew. Sustain. Energy Rev.* **2017**, *78*, 176–193. [CrossRef]
9. Kalbasi, R.; Alemrajabi, A.A.; Afrand, M. Thermal modeling and analysis of single and double effect solar stills: An experimental validation. *Appl. Therm. Eng.* **2018**, *129*, 1455–1465. [CrossRef]
10. Tsilingiris, P.T. The application and experimental validation of a heat and mass transfer analogy model for the prediction of mass transfer in solar distillation systems. *Appl. Therm. Eng.* **2013**, *50*, 422–428. [CrossRef]
11. Shoeibi, S.; Rahbar, N.; Esfahlani, A.A.; Kargarsharifabad, H. A review of techniques for simultaneous enhancement of evaporation and condensation rates in solar stills. *Sol. Energy* **2021**, *225*, 666–693. [CrossRef]
12. Estahbanati, M.R.K.; Ahsan, A.; Feilizadeh, M.; Jafarpur, K.; Ashrafmansouri, S.S.; Feilizadeh, M. Theoretical and experimental investigation on internal reflectors in a single-slope solar still. *Appl. Energy* **2016**, *165*, 537–547. [CrossRef]
13. Afrand, M.; Kalbasi, R.; Karimipour, A.; Wongwises, S. Experimental investigation on a thermal model for a basin solar still with an external reflector. *Energies* **2017**, *10*, 18. [CrossRef]
14. Kabeel, A.E.; Sathyamurthy, R.; Sharshir, S.W.; Muthumanokar, A.; Panchal, H.; Prakash, N.; Prasad, C.; Nandakumar, S.; El Kady, M.S. Effect of water depth on a novel absorber plate of pyramid solar still coated with TiO₂ nano black paint. *J. Clean. Prod.* **2019**, *213*, 185–191. [CrossRef]
15. Sharshir, S.W.; Peng, G.; Wu, L.; Yang, N.; Essa, F.A.; Elsheikh, A.H.; Mohamed, S.I.T.; Kabeel, A.E. Enhancing the solar still performance using nanofluids and glass cover cooling: Experimental study. *Appl. Therm. Eng.* **2017**, *113*, 684–693. [CrossRef]
16. Amarloo, A.; Shafii, M.B. Enhanced solar still condensation by using a radiative cooling system and phase change material. *Desalination* **2019**, *467*, 43–50. [CrossRef]
17. Kumar, R.A.; Esakkimuthu, G.; Murugavel, K.K. Performance enhancement of a single basin single slope solar still using agitation effect and external condenser. *Desalination* **2016**, *399*, 198–202. [CrossRef]
18. Sharshir, S.W.; Elsheikh, A.H.; Edreis, E.M.A.; Ali, M.K.A.; Sathyamurthy, R.; Kabeel, A.E.; Zang, J.; Yang, N. Improving the solar still performance by using thermal energy storage materials: A review of recent developments. *Desalin. Water Treat.* **2019**, *165*, 1–15. [CrossRef]
19. Katekar, V.P.; Deshmukh, S.S. A review of the use of phase change materials on performance of solar stills. *J. Energy Storage* **2020**, *30*, 101398. [CrossRef]
20. Omara, A.A.M.; Abuelnuor, A.A.A.; Mohammed, H.A.; Khiadani, M. Phase change materials (PCMs) for improving solar still productivity: A review. *J. Therm. Anal. Calorim.* **2020**, *139*, 1585–1617. [CrossRef]
21. Yousef, M.S.; Hassan, H. Energetic and exergetic performance assessment of the inclusion of phase change materials (PCM) in a solar distillation system. *Energy Convers. Manag.* **2019**, *179*, 349–361. [CrossRef]
22. Chaichan, M.T.; Kazem, H.A. Single slope solar distillator productivity improvement using phase change material and Al₂O₃ nanoparticle. *Sol. Energy* **2018**, *164*, 370–381. [CrossRef]
23. Kabeel, A.E.; Abdelgaied, M.; Eisa, A. Effect of graphite mass concentrations in a mixture of graphite nanoparticles and paraffin wax as hybrid storage materials on performances of solar still. *Renew. Energy* **2019**, *132*, 119–128. [CrossRef]
24. Radomska, E.; Mika, L.; Sztokler, K. The Impact of Additives on the Main Properties of Phase Change Materials. *Energies* **2020**, *13*, 3064. [CrossRef]
25. Shalaby, S.M.; El-Bialy, E.; El-Sebaei, A.A. An experimental investigation of a v-corrugated absorber single-basin solar still using PCM. *Desalination* **2016**, *398*, 247–255. [CrossRef]
26. Sonker, V.K.; Chakraborty, J.P.; Sarkar, A.; Singh, R.K. Solar distillation using three different phase change materials stored in a copper cylinder. *Energy Rep.* **2019**, *5*, 1532–1542. [CrossRef]
27. Mousa, H.; Naser, J.; Gujarathi, A.M.; Al-Sawafi, S. Experimental study and analysis of solar still desalination using phase change materials. *J. Energy Storage* **2019**, *26*, 100959. [CrossRef]

28. Al-Harshsheh, M.; Abu-Arabi, M.; Ahmad, M.; Mousa, H. Self-powered solar desalination using solar still enhanced by external solar collector and phase change material. *Appl. Therm. Eng.* **2022**, *206*, 118118. [CrossRef]
29. Mousa, H.; Gujarathi, A.M. Modeling and analysis the productivity of solar desalination units with phase change materials. *Renew. Energy* **2016**, *95*, 225–232. [CrossRef]
30. Kateshia, J.; Lakhera, V.J. Analysis of solar still integrated with phase change material and pin fins as absorbing material. *J. Energy Storage* **2021**, *35*, 102292. [CrossRef]
31. Tabrizi, F.F.; Dashtban, M.; Moghaddam, H. Experimental investigation of a weir-type cascade solar still with built-in latent heat thermal energy storage system. *Desalination* **2010**, *260*, 248–253. [CrossRef]
32. Sarhaddi, F.; Tabrizi, F.F.; Zoori, H.A.; Mousavi, S.A.H.S. Comparative study of two weir type cascade solar stills with and without PCM storage using energy and exergy analysis. *Energy Convers. Manag.* **2017**, *133*, 97–109. [CrossRef]
33. Fu, H.; Dai, M.; Song, H.; Hou, X.; Riaz, F.; Li, S.; Yang, K.; Ali, I.; Peng, C.; Sultan, M. Updates on evaporation and condensation methods for the performance improvement of solar stills. *Energies* **2021**, *14*, 7050. [CrossRef]
34. Radomska, E.; Mika, L.; Sztekler, K.; Kalawa, W. Experimental validation of the thermal processes modeling in a solar still. *Energies* **2021**, *14*, 2321. [CrossRef]
35. Zbińkowski, P.; Zmywaczyk, J.; Koniorczyk, P. Experimental investigations of thermophysical properties of some paraffin waxes industrially manufactured in Poland. *AIP Conf. Proc.* **2017**, *1866*, 40044. [CrossRef]
36. Ministerstwo Inwestycji i Rozwoju. Dane do Obliczeń Energetycznych Budynków. Available online: <https://archiwum.miir.gov.pl/strony/zadania/budownictwo/charakterystyka-energetyczna-budynkow/dane-do-obliczen-energetycznych-budynkow-1/> (accessed on 30 January 2020).
37. Simo-Tagne, M.; Zoulalian, A.; Rémond, R.; Rogaume, Y. Mathematical modelling and numerical simulation of a simple solar dryer for tropical wood using a collector. *Appl. Therm. Eng.* **2018**, *131*, 356–369. [CrossRef]
38. Simo-Tagne, M.; Tagne, A.T.; Ndukwu, M.C.; Bennamoun, L.; Akong, M.B.O.; El Marouani, M.; Rogaume, Y. Numerical Study of the Drying of Cassava Roots Chips Using an Indirect Solar Dryer in Natural Convection. *AgriEngineering* **2021**, *3*, 138–157. [CrossRef]
39. Simo-Tagne, M.; Ndukwu, M.C.; Zoulalian, A.; Bennamoun, L.; Kifani-Sahban, F.; Rogaume, Y. Numerical analysis and validation of a natural convection mix-mode solar dryer for drying red chilli under variable conditions. *Renew. Energy* **2020**, *151*, 659–673. [CrossRef]
40. Elango, C.; Gunasekaran, N.; Sampathkumar, K. Thermal models of solar still—A comprehensive review. *Renew. Sustain. Energy Rev.* **2015**, *47*, 856–911. [CrossRef]
41. Cengel, Y. *Heat and Mass Transfer: A Practical Approach*; McGraw-Hill: Singapore, 2006.
42. Incropera, F.P.; DeWitt, D.P.; Bergman, T.L.; Lavine, A.S. *Fundamentals of Heat and Mass Transfer*; John Wiley & Sons: Hoboken, NJ, USA, 2007.
43. Tiwari, G.N.; Tiwari, A. *Handbook of Solar Energy. Theory, Analysis and Applications*; Springer: Singapore, 2016. ISBN 978-981-10-0807-8.
44. Mirsadeghi, M.; Cóstola, D.; Blocken, B.; Hensen, J.L.M. Review of external convective heat transfer coefficient models in building energy simulation programs: Implementation and uncertainty. *Appl. Therm. Eng.* **2013**, *56*, 134–151. [CrossRef]
45. Dinçer, İ.; Zamfirescu, C. Appendix B Thermophysical Properties of Water. In *Drying Phenomena: Theory and Applications*; John Wiley & Sons: Hoboken, NJ, USA, 2016; pp. 457–459.
46. Tsilingiris, P.T. Thermophysical and transport properties of humid air at temperature range between 0 and 100 °C. *Energy Convers. Manag.* **2008**, *49*, 1098–1110. [CrossRef]
47. Tsilingiris, P.T. Review and critical comparative evaluation of moist air thermophysical properties at the temperature range between 0 and 100 °C for Engineering Calculations. *Renew. Sustain. Energy Rev.* **2018**, *83*, 50–63. [CrossRef]
48. Cheng, W.L.; Huo, Y.K.; Nian, Y. Le Performance of solar still using shape-stabilized PCM: Experimental and theoretical investigation. *Desalination* **2019**, *455*, 89–99. [CrossRef]
49. The Properties of Stainless Steel. Available online: <https://www.alfa-tech.com.pl/stal-nierdzewna-h17-x6cr17-14016-430> (accessed on 4 December 2020).
50. The Properties of Glass. Available online: <https://www.continentaltrade.com.pl/szklo-sodowo-wapniowe> (accessed on 4 December 2020).
51. Luyt, A.S.; Krupa, I. Thermal behaviour of low and high molecular weight paraffin waxes used for designing phase change materials. *Thermochim. Acta* **2008**, *467*, 117–120. [CrossRef]
52. Khalifa, A.J.N.; Hamood, A.M. Effect of insulation thickness on the productivity of basin type solar stills: An experimental verification under local climate. *Energy Convers. Manag.* **2009**, *50*, 2457–2461. [CrossRef]

Disclaimer/Publisher’s Note: The statements, opinions and data contained in all publications are solely those of the individual author(s) and contributor(s) and not of MDPI and/or the editor(s). MDPI and/or the editor(s) disclaim responsibility for any injury to people or property resulting from any ideas, methods, instructions or products referred to in the content.